

BACHELORTHESIS

Sensor Driven Topology-Optimization for Additively Manufactured Humanoid Robotic Parts

vorgelegt von

Julian Deinert

MIN-Fakultät

Fachbereich Informatik

Technische Aspekte Multimodaler Systeme

Studiengang: Informatik

Matrikelnummer: 6535880

Erstgutachter: Dr. Norman Hendrich

Zweitgutachter: Florens Wasserfall

Abstract

The current design of robotic parts of the Bit-Bots Wolfgang robot is very simplistic. Also the availability of off-site manufactured parts is not ideal. This work proposes a method of optimizing the topology of robotic parts based on data, acquired from a force torque sensor, motor currents and simulations. The optimized legs and feet were printed using a standard low-cost fused deposition modelling printer and tested on the robot.

The finished parts show no obvious impaired performance compared to the original parts but are significantly lighter and faster to obtain. The optimized topology also uses less material and takes therefore less time to print.

Zusammenfassung

Das gegenwärtige Design von Roboterteilen des Wolfgang Roboters des Bit-Bots Teams ist sehr simpel. Zusätzlich ist die Verfügbarkeit von auswärts-gefertigten Teilen nicht ideal. Diese Arbeit präsentiert eine Methode, Roboterteile basierend auf Sensordaten aus Motorströmen, einem Kraft-Drehmoment-Sensor und Simulationen, hinsichtlich ihrer Topologie zu optimieren. Die optimierten Füße und Beine wurden mit Hilfe eines standard FDM 3D-Druckers gedruckt und am Roboter getestet.

Die fertiggestellten Teile zeigten keine offensichtlichen Nachteile in ihrer Leistung verglichen mit den original Teilen. Jedoch sind die optimierten Teile deutlich leichter und schneller verfügbar. Die optimierte Topologie spart außerdem Material ein, wodurch die Druckzeit weiter gesenkt werden konnte.

List of Figures

1	Feet of the Wolfgang robot made from a square aluminum base plate	1
2	Wolfgang robot standing on artificial lawn	3
3	Data captured while the robot is falling from a height of one meter	15
4	Section of the collected servo motor data in the left ankle roll motor showing a peak effort of 6.49 Nm	17
5	3D-printed foot with a top and bottom part which are connected by an ATI Mini45 f/t-sensor	19
6	3D-printed foot with closer look at an ATI Mini45 f/t-sensor connecting the top and bottom part	20
7	3D-printed leg split in the middle with an ATI Mini45 f/t-sensor connecting the two parts	21
8	Front view of a 3D-printed leg split in the middle with an ATI Mini45 f/t-sensor connecting the two parts	22
9	Graph showing the force and torque inside the knee of the robot over multiple steps with annotated events	23
10	Graph showing the forces inside the knee of the robot over multiple steps with sum of all axes' forces	23
11	Graph showing the force and torque inside the left foot of the robot over multiple steps with annotated events	26
12	ANSYS Workbench table showing the material properties for PLA	28
13	Workflow elements as seen in the ANSYS Workbench showing links between different steps of the optimization process	29
14	Side view of the lower right leg with mounting holes for a servo motor	31
15	Front view of the leg with motor-models to verify cutout dimensions	32
16	Rotated leg to check for possible collision with the servo motors	33

17	Leg attached to a 3d-model of the foot with simplified motor-axes	34
18	Walk ready pose of the Wolfgang robot	35
19	Back view of the modeled leg with faces selected for the forces in red	36
20	Back view of the modeled leg with faces selected for the torque in red	37
21	Forces defined to be acting on the top axis of the modeled leg	38
22	Torques defined to be acting on the center of the modeled leg .	38
23	Distribution of stress in the material of the leg	39
24	Distribution of deformation in the material of the leg	39
25	Back view of the leg showing design-regions in blue and exclusion-regions in red	40
26	Raw response of the topology optimization of the lower leg . .	41
27	Optimized topology of the leg showing small disconnected facets highlighted in orange	42
28	Optimized topology with important features to retain highlighted in blue	43
29	Optimized leg after smoothing	44
30	Front view of the optimized lower leg with foot and motors . .	45
31	3D-model of the foot designed to use the maximum amount of space available	47
32	Bottom view of a 3D-model of the foot designed to use the maximum amount of space available	48
33	Model of the foot with cutouts and forward tilted leg to show possible collisions	49
34	Distribution of stress inside the foot of the robot	50
35	Distribution of deformation inside the foot of the robot	51
36	Design regions in blue and exclusion regions in red, defined for the foot for the topology optimization process	52
37	Raw result of the optimization for the foot	53
38	Models of the optimized lower leg and the optimized foot with motors	54

39	Side view of the printed optimized foot showing the connection to the leg	55
40	Front view of the printed optimized foot mounted on the optimized lower leg	56
41	The Prusa i3 FDM-printer printing one of the first layers of an optimized foot	57
42	Printed optimized leg with support material already removed .	58
43	Printed optimized foot with screw holes of alternating depths making it impossible to mount	59
44	Optimized foot with very thin structure connecting the front and back section	60
45	Optimized foot with only 15% mass retention setting mounted on the robot for a walking test	61
46	Optimized leg and foot mounted on the servo motors of the foot resembling a complete lower leg	63
47	Optimized leg and foot mounted on the robot next to an unmodified leg	64

List of Tables

1	Force and torque inside the knee of the robot over 1.8 seconds with a resolution of 0.1s	24
2	Force and torque inside the foot of the robot over 1.8 seconds with a resolution of 0.1s	25
3	Data about the volume, weight, used filament and print time of the optimized foot and leg of the robot	62
4	Comparison of weight and the time it takes to obtain the part of the optimized and unaltered leg of the robot	62
5	Comparison of weight and the time it takes to obtain the part of the optimized and unaltered foot of the robot	62

Acronyms

ROS Robot Operating System

3D three dimensional

FDM Fused Deposition Modeling

SLA Stereolithography

SLS Selective Laser Sintering

SLM Selective Laser Melting

PLA Polylactic acid

ABS Acrylonitrile butadiene styrene

UV ultra violet

AM additive manufacturing

FEA Finite Element Analysis

FEM Finite Element Method

CAD Computer Assisted Design

SIMP Solid Isotropic Material with Penalisation

STL stereolithography

Contents

Abstract	i
Zusammenfassung	i
List of Figures	iv
List of Tables	v
Acronyms	vi
1 Introduction	1
1.1 Motivation	2
2 Related Work	5
3 Fundamentals	9
3.1 Additive Manufacturing	9
3.1.1 Fused Deposition Modeling (FDM)	10
3.1.2 Stereolithography (SLA)	11
3.1.3 PolyJet/Multijet	11
3.2 Finite Element Method and Analysis	12
3.3 Topology Optimization	13
4 Topology Optimization of Robotic Parts	15
4.1 Acquisition and Analysis of Forces	15
4.1.1 Simulation using ROS and the Gazebo Framework	15
4.1.2 Using the Stall Torque as an Upper Limit	16
4.1.3 Measuring the Motor Effort to Derive Forces	17
4.1.4 Measuring Forces and Torques using an ATI Mini45 F/T-Sensor	18
4.1.5 Analysis of Forces	18
4.2 Tools Used	27
4.2.1 ANSYS Workbench Suite	27
4.2.2 Slic3r	28

4.2.3	Prusa i3	29
4.3	Topology Optimization of the Lower Right Leg	30
4.3.1	Modeling the Leg	30
4.3.2	Simulating the Leg under Load	31
4.3.3	Optimizing the Topology of the Leg	33
4.4	Topology Optimization of the Foot	46
5	Manufacturing the Optimized Parts using Additive Manufacturing	57
6	Results	59
7	Conclusion	65
7.1	Outlook	65

1 Introduction

In 2015, the Bit-Bots team of the University of Hamburg developed a three dimensional (3D)-printable humanoid robot, called the Hambot. While the Hambot project was successful and the robot was actively used by the team, the mechanical design was mainly done manually, so that the result mainly consists of simple geometric shapes (TAMS 2017).



Figure 1: Feet of the Wolfgang robot made from a square aluminum base plate

This thesis aims to provide an efficient approach on producing different parts of the robot on-site using a low-cost Fused Deposition Modeling (FDM) 3D printer and a topology optimization process to optimize the parts based on gathered information about forces acting on the parts of the *Wolfgang robot*.

1.1 Motivation

Since additive manufacturing (AM) is used to produce a significant part of the robot, experimenting with different and geometrically complex parts can be done with very little effort (Berman, 2012). In order to adapt the shape of certain parts to their function in the finished robot, topology optimization can be used to iteratively optimize a part concerning real world constraints (Brackett et al., 2011). This is done by applying finite element methods and analysis based on load conditions to simulate physical forces a part has to withstand (Zegard et al., 2016). Optimized legs could lead to better walking performance, improved stability or weight reduction (Brackett et al., 2011, p. 351). Additionally, reduced volume or mass of the 3D- printed parts lead to shorter reproduction times, further increasing the value of AM for parts. Lastly, optimized parts might also reveal better placement options for motors and cables, so that space is used more efficiently. In order to successfully optimize the topology of a part, it is necessary to define real-world load constraints for the part. Loads that are of interest, are static loads, which typically occur when the robot stands still on one or both feet or moves in a predefined way. Load peaks, which may happen when the robot falls over or moves in other non-predefined ways, are worth observing as well (Sardain et al., 2004). In order to measure these forces there are basically four approaches. One is to calculate static loads from measurements of the parts of the robot, using the laws of physics. Another is to read forces off of the force feedback which is provided by the servo-motors of the robot. Similarly, force data can be acquired using the Robot Operating System (ROS)-framework in combination with the gazebo simulation framework, which provides measurements for various forces (Koenig et al., 2004). Finally, forces can be measured using 6-axis force-torque sensors, which can be mounted anywhere on the robot using a 3D-printed platform (ATI Industrial Automation Manual 2016).

Ultimately, the analysis of forces being exerted on the robot, while walking or falling, provides valuable data for other optimization not limited to

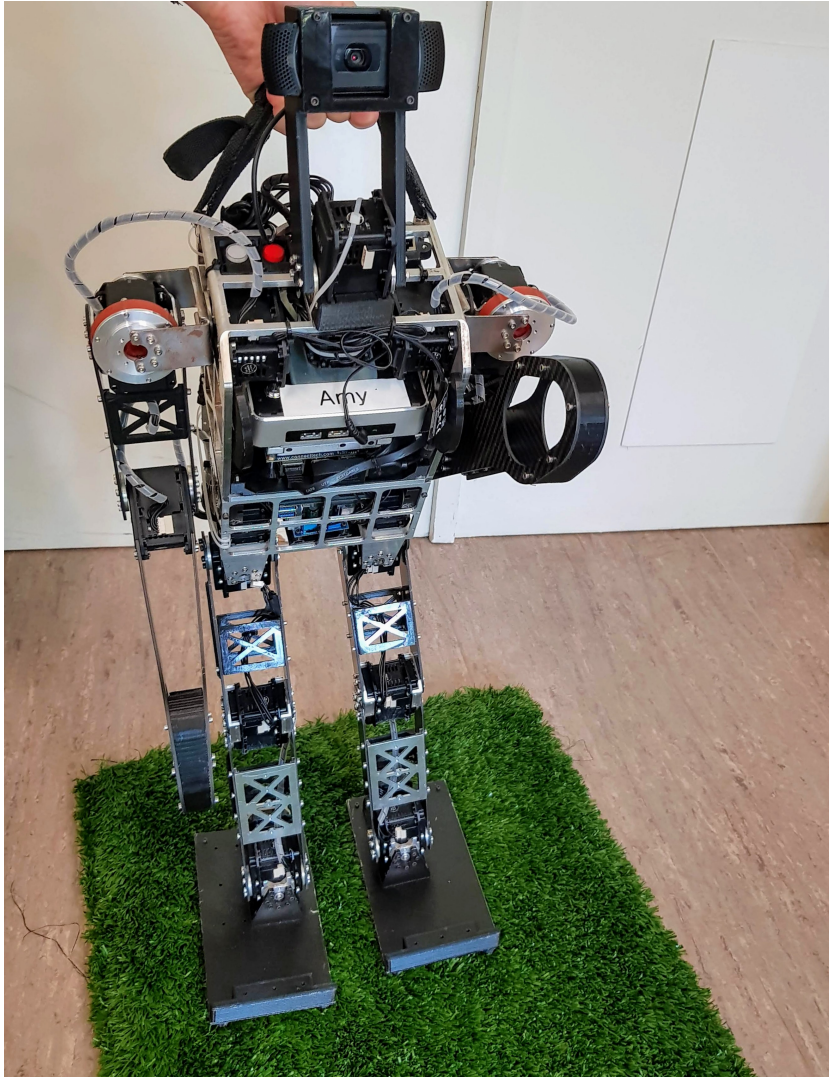


Figure 2: Wolfgang robot standing on artificial lawn

topology optimization but to the overall performance of the robot.

2 Related Work

The topic of this thesis relates to three larger topics. Topology optimization, 3D-printing and robotics, all of which are heavily linked in the process of creating optimized parts. Topology optimization is already widely used for different types of manufacturing. Popular examples are casting and machining. A key aspect of topology optimization is, that it solves a material distribution problem by producing shapes that are often different from what a traditional design process would turn up. This leads to sometimes very fine structures, which are not suitable for processing techniques like casting or machining, mainly due to accessibility issues. For AM approaches however, there are no limitations for the manufacturing process except the minimum feature size at which structures are still manufacturable. (Brackett et al., 2011) concluded that the main limitation for manufacturing topology optimized parts is no longer within the manufacturing stage, when using AM approaches, but within the design stage. The reason for this is that topology optimization uses a lot of constraints which are implemented as design variables to keep track of the optimization progress. D. Brackett et. al. propose different approaches to reduce the total number of variables, while retaining the same or better results. One is to eliminate elements that have been unaltered for a number of iterations by the solver. This, however, bears the problem that elements, once eliminated, can't be re-added to the solver, which could prevent optimal solutions. Another approach is to refine the mesh dynamically where a finer mesh is needed. All in all, an increase in computational complexity of the topology optimization process is only justifiable in cases where a small optimization has a rather big impact, such as in aviation technology.

Other, newer, works mention, that post processing of the generated designs is often necessary and limits the use of topology optimization even when using AM as the production method (Zegard et al., 2016)(X. Wang et al., 2016).

Furthermore, the quality of additively manufactured parts varies, due to minimal shrinking and warping effects during cooling. This can lead to

inconsistencies in material strength, structure or overall form (Torries et al., 2017).

For the purpose of reducing material while maintaining structural strength, Wang et al. proposed a method of optimizing the infill of 3D-printed parts. Their approach involves optimizing the infill-pattern by generating a skin-frame-structure. The structure ensures stiffness and stability while removing a great portion of the part's volume. The generation of the skin-frame-structure is automated and utilizes an optimization process in order to reduce the number of struts in the structure. The final skin-frame-structure is geometrically approximate to the original meshed body but reduces total volume by around 33% (W. Wang et al., 2013).

In the field of manufacturing robotic parts, AM is not yet heavily integrated. The Hambot, which was developed at the University of Hamburg, resembles a humanoid robot with several 3D-printed parts. This is due to the main goals of the Hambot-project, which were to lower the cost, increase simplicity of humanoid robots in order to enable new teams to get into robocup soccer and make interactions with the robot more productive. AM plays a rather large role in accomplishing these goals, as it enables teams to manufacture their own parts on low-cost FDM-printers (Bestmann et al., 2015).

Besides projects that aim at printing complete robots like the Hambot, there are also smaller components of the robot that can be manufactured additively. In 2017 Wasserfall et al. developed a 3D-printed force-sensor for use in robotic feet. The basic principle behind the sensor was to utilize the mechanical properties of Polylactic acid (PLA)-plastic to calibrate a proximity sensor in order to report a force acting on the material. The sensors were used in the contact points of humanoid robotic feet.

Due to the simplicity of the sensor, its inexpensive components and the use of 3D-printing, the cost of one sensor of around \$24 was significantly lower than commercially available sensors (Wasserfall et al., 2017).

In terms of designing robots so that, they look more human, various manually designed approaches exist. Hild et al., 2012 designed a modular robot called Myon, that can be reassembled while it actively operates. The design

of the limbs and torso feature curved surfaces, which makes the robot look more human. Also the head features a single centered camera, resembling an eye. The robot is quite robust, as it is supported by very sturdily build parts which the authors refer to as an exoskeleton.

In contrast to the quite clean appearance of the Myon robot, the Poppy robot designed by Lapeyre, 2014 features a more bone-like structure. All the parts of the Poppy robot are 3D-printed and therefore quite easy to obtain. The limbs are composed of four main struts with little cross-hatched strut-patterns between the main struts. This enhances support and saves a lot of weight, as the robot only weighs 3.5 kg at a height of 85cm.

As mentioned before, topology optimization is especially useful, where a small optimization results in a large improvement of the performance of a part. This is for example the case with wing boxes of planes manufactured by Airbus. Krog et al., 2004 present two approaches on optimization of a wing box rib structure, to lower the weight of airplane wings. The ribs of the wing box only carry a small amount of the overall weight of the wing as well as only a small percentage of the loads which act on a wing. Therefore the wings were an optimal candidate for topology optimization used in highly redundant structures.

3 Fundamentals

This section gives an overview over the technologies used to optimize and manufacture the robotic parts in this thesis.

3.1 Additive Manufacturing

Traditional manufacturing techniques such as machining or casting have been around for as long as 6000 years (Ravi, 2005). They are well embedded in mass production processes and are suitable for a wide range of materials. These production methods are a good fit for large scale operations but lack necessary features when it comes to smaller and more fast-moving production schedules. The process of casting requires a mold that has to be manufactured beforehand. This limits the ability to quickly adapt the design of the prototype to all kinds of changes. When dealing with machining processes, the initial costs are often quite high so that prototyping on those machines is economically challenging.

The approach of AM tries to solve those limitations. The main idea is to create the final product by producing one layer at a time. Layers of material are added on top of each other, while fusing them using different approaches depending on the manufacturing technology used. AM can utilize a wide range of materials, like poly-carbonates for example, which keeps material costs at bay. Additionally, this manufacturing method can produce completely different products without altering the setup. Only the input file needs to be changed. This makes it perfectly suitable for rapid prototyping. AM furthermore doesn't suffer from the limitations that big machining equipment or casting processes do. Since material is being layered on top of itself there are far fewer accessibility issues with AM than there would be with casting or machining. Additionally, machines for AM are often much less expensive than CNC-machines for example. This makes AM a promising technology when considering the production of prototypes.

For all AM techniques a 3D-model of the object is required. The model is sliced into layers with a predetermined thickness by a slicer and then translated into control-commands for the machine, which describe where it should

depose material and also where support structures are needed. For some types of AM, an infill can be specified. The infill describes how the structure of the inner filling of the object should be constructed. There are different types of infills with different advantages. All settings for the slicer can be tweaked to achieve an optimal result. The basic principle of AM can be applied to different materials. In order to make a wide range of materials behave in a way that allows them to be layered, different approaches have been developed (*Design Guide: Fused Deposition Modeling* n.d.)(Palermo, 2013).

3.1.1 Fused Deposition Modeling (FDM)

FDM utilizes a print-head that extrudes material onto a hot-bed, which is simply a heated plate. The print-head consists of a, often geared, feeding mechanism to push material through a nozzle which is heated to suitable temperatures. The material is melted right before being extruded onto the hot-bed. FDM is typically used for materials with a low melting temperature such as PLA or Acrylonitrile butadiene styrene (ABS). The print head is moved in x-, y-, z-direction either actively or passively. This depends on the arrangement of the motors, which often are mounted in a way, so that for example the print head is moved along one axis and the hot-bed can move on the remaining two axes. This is often decided based on structure and space limitations of the machine to increase stability. FDM-printers that use ABS also feature a heated chamber. This is necessary as ABS retracts and shrinks while cooling. To ensure that the finished product retains its shape and can cool down consistently, the chamber is kept at around 80°C for the complete duration of the manufacturing process. FDM is often associated with the term 3D-printing. The produced objects of FDM-printers often show the single layers of material. Also, the objects are significantly more stable when stressed in the direction of the layers. Objects are often strategically rotated and positioned in the slicer before production, to increase the success rate of prints and increase the stability of the finished product (*Design Guide: Fused Deposition Modeling* n.d.).

3.1.2 Stereolithography (SLA)

While FDM utilizes a print head system to build a 3D-object from bottom to top, Stereolithography (SLA) uses an ultra violet (UV) light source to solidify spots in a polymer liquid. The polymer liquid is spread out very thinly on a translucent plate. A UV light is then pointed at the locations where material is needed. This solidifies the liquid which then adheres to the base plate. The base plate is moved up a few millimeters after every layer. The setup time for SLA-printers is basically the same as it is for FDM-printers, although setting up a SLA-printer involves a lot more precision and care than the setup for a FDM print job. For every print job, a reservoir which holds the polymer liquid needs to be installed inside the printer. After the reservoir has been installed, the build plate of the printer can be placed on top of the reservoir. After both steps are completed, the polymer liquid can be poured into the reservoir. All of these steps have to be executed very carefully to ensure the success of a print job (Hull, 1984).

3.1.3 PolyJet/Multijet

PolyJet or Multijet printers are capable of producing prints with very high resolution. This is attributable to their design. Simply put, a Multijet printer resembles an ink-jet printer with an additional z-axis. This enables the print head to move up after each printed layer, thus creating a 3D object. The material which is used by the printer, as with the SLA-printer, is a polymer resin, that is hardened through the use of an UV light source. The print head typically consists of multiple nozzles, that can print independent materials and colors at the same time. In addition to the resin, the print head is also capable of printing a wax-like support material simultaneously. This further improves the quality and possible resolution of printed objects. The support structure can later be melted away in a calibrated oven, at a temperature of 69°C, due to its low melting point. The print time of objects on the Multijet is mainly determined by the height of the object, since the printer always does a full pass over the entire print surface. Material- and overall maintenance-cost is significantly higher than those of SLA- or FDM-printers, which renders the

Multijet printer less suited for rapid prototyping. Typically, Multijet printers are used to produce objects with extremely fine details and smooth surfaces, such as prototypes that are meant to resemble a finished design, precise molds and other objects with very tight tolerance margins.

3.2 Finite Element Method and Analysis

The method of finite elements offers an approach to solve mathematical problems approximately that would otherwise be unsolvable. This is achieved by dividing the problem into a finite number of sub-problems, each with a computable mathematical solution. Finite Element Method (FEM) or Finite Element Analysis (FEA) is often used to analyze structures under load. At first, boundary and load conditions for the structure are defined. The structure is then divided into smaller segments, all of the same type. Typically a simple geometrical shape such as a triangle or a rectangle is used. The shape of each element is defined by a simple function. This ensures that the displacement under load for the element is a calculable problem and can be solved for every element. The process of dividing the model into a finite number of elements is called meshing. After the meshing is done, a relationship $\{f\}_i = [k]_i \{d\}_i$ is defined for every Element i of the model, where $\{f\}$ is the nodal load vector, $\{d\}$ is the nodal displacement vector and $[k]$ denotes the stiffness matrix for the element. This equation describes the displacement of all the nodes of an element given all their loads. All the relationships of the elements are then linked through continuity constraints to postulate the equation for the whole model. $\{F\} = [K]\{D\}$ describes the loads of every node in the whole model given the displacements and stiffness matrix for every node in the model. Since usually most of the loads and all of the stiffnesses are known, the equation needs to be solved for the displacements. This is achieved by building the inverse of the stiffness matrix $[K]$. The displacement depending on the loads and the stiffness matrix can therefore be described by $\{D\} = [K]^{-1}\{F\}$. If the stiffness matrix is singular, there is no unique solution to the FEA. After a solution for the global equation is found, the results then have to be interpolated for every element, in order to

determine displacements for the elements.

Besides structural analysis, FEA is also used in fluid dynamics, electrostatic analyses as well as in the analyses of heat conduction.

3.3 Topology Optimization

Topology optimization is a mathematical approach to optimize the distribution of a material, given various constraints such as load, design space and other boundary conditions (Sigmund et al., 2013). The goal achieved by topology optimization is to maximize a the performance of a part concerning predefined conditions. In general, topology optimization optimizes for minimal compliance or flexibility which in return maximizes stiffness. This often leads to very abstract designs, which are often hard to manufacture using traditional manufacturing methods. Although AM mitigates a lot of manufacturing restrictions, optimized parts are usually post-processed manually, where structures are simplified and revised to meet manufacturing constraints.

Topology optimization is an iterative process where in each iteration the previously generated optimized structure is used as the new baseline for the next iteration. Every topology optimization task can be written in the usual form of an optimization problem.

$$\begin{aligned}
 & \underset{x}{\text{minimize}} && F = F(\mathbf{u}(\rho), \rho) = \int_{\Omega} f(\mathbf{u}(\rho), \rho) dV \\
 & \text{subject to} && G_0(\rho) = \int_{\Omega} \rho dV - V_0 \leq 0 \\
 & && G_j(\mathbf{u}(\rho), \rho) \leq 0 \text{ with } j = 1, \dots, m
 \end{aligned} \tag{1}$$

Where the distribution of material is denoted by the design variable ρ_e for every element and can take any value between 0 and 1, where 0 is denoting no material and 1 meaning the presence of material. The optimization is subjected to a number of constraints between 1 and m . Since values different from 0 and 1 are not advantageous for the distribution of material, a penalization is often used, to steer the optimization to a binary solution.

This interpolation is usually implemented using the Solid Isotropic Material with Penalisation (SIMP) method. It uses a power law to penalize values between 0 and 1 in compliance, hence rendering them unreasonable for the optimization process. The power law is expressed as $E(\rho_0) = \rho_e^p E_0$ given a $p > 1$. Too low or too high values of p may cause too little penalization, and therefore too many in-between values. If p is set too high, the optimization often converges to local minima. The proper value for p is widely believed to be $p = 3$ (Sigmund et al., 2013).

4 Topology Optimization of Robotic Parts

Before a 3D-model of a robotic part can be optimized, various constraints have to be set. For the optimization to be successful, these constraints are set by first simulating and analyzing the behaviour of the robot.

4.1 Acquisition and Analysis of Forces

In order to measure various forces in the robot, it is necessary to use a force-torque sensor. To ensure that a real robot or the sensor would not be damaged by a test run, a simulation of the robot is used. This simulation is performed by using the gazebo framework paired with ROS to control the robot and retrieve data.

4.1.1 Simulation using ROS and the Gazebo Framework

A force-torque sensor is placed inside the knee joint of the right leg. It reports data about the force and torque being exerted on the right knee joint. In order to get a load peak, the robot is elevated to one meter above the ground and then falls, accelerated by gravity. On impact with the ground the force-torque sensor reports data, shown in Figure 3.

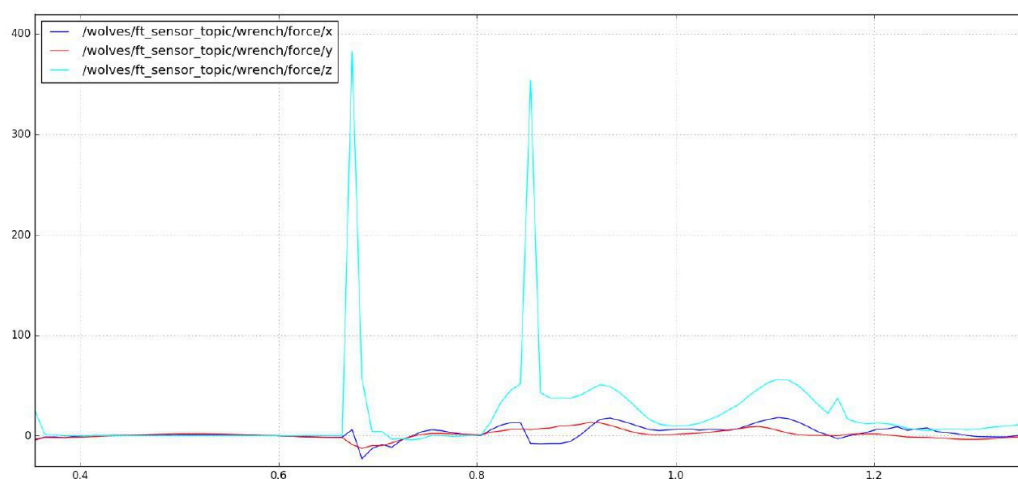


Figure 3: Data captured while the robot is falling from a height of one meter

The plot shows, that a peak force of about 370 N is experienced by the knee joint in this scenario. Although the peak force seems to be well defined, it is possible that the real peak was not captured due to the resolution of the sensor. Therefore, the real peak force might be much higher. In order to check for this kind of error, the sample rate of the force-torque sensor is increased to 1000 Hz. Upon rerunning the simulation, a force peak of roughly 2200 N is observed, confirming the theory.

Another problem about the simulation is, that the walking movements of the robot cannot be simulated very accurately. In some cases, collisions of the feet with the floor result in bouncy movements of the robot, often leading to the robot falling over. Additionally, the simulation only gives limited information about the forces really being exerted on a joint. Because of the reasons outlined, I decided to consider the findings of the simulation as baseline values for further investigations.

4.1.2 Using the Stall Torque as an Upper Limit

One of the problems with robots falling over is the damage to parts when a robot hits the ground. Besides parts like arms or legs, which can be replaced rather easily and inexpensively, the motors of the robot are prone to damage as well. Even more so, if the arms or legs, which are attached to the motors, are increased in stability. Damage to the motor is often experienced as teeth breaking off of the gearbox of the motor. This damages the transmission of the motor beyond repair, which then have to be replaced. Since this is rather expensive, it is desirable, that an arm or leg would break before damage to the transmission of the motor can occur.

A guideline to under which load a part should break to prevent damage to a motor is the maximum torque the motor can produce while unable to turn. This is called the stall torque. Motors are typically designed to withstand slightly higher loads than the stall torque. An optimized part should therefore break under a load slightly above the stall torque of the motors it is attached to. The stall torque also gives an idea of how much force a part typically has to withstand. For that reason the stall torque can also be used as a baseline

for a stability-focused optimization.

4.1.3 Measuring the Motor Effort to Derive Forces

While the robot is walking, the servo-motors are publishing various values about their current performance. These values can be recorded and used to derive forces acting in the joints of the robot. This is made possible due to the linear correlation between amperage drawn by the motor and its produced torque in Nm (Robotis 2009). The values are recorded into a *rosbag*. Rosbag is a special file created by ROS that enables the user to later replay the data captured in real time, in order to observe the values more closely. Figure

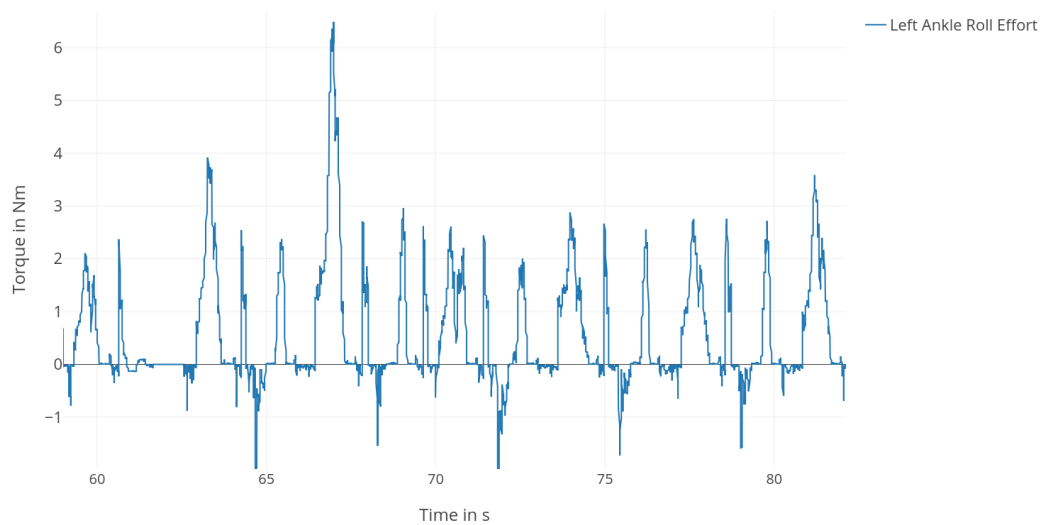


Figure 4: Section of the collected servo motor data in the left ankle roll motor showing a peak effort of 6.49 Nm

4 shows a section of a 137s recording of torques in the left ankle roll servo motor, which is the motor connected to the back of the left foot of the robot. The graph shows an average torque of about 3.2 Nm as well as a peak torque of about 6.5 Nm.

4.1.4 Measuring Forces and Torques using an ATI Mini45 F/T-Sensor

In order to acquire more precise measurements a force-torque-sensor is used to measure forces and torques which occur inside the foot and leg of the robot. The sensor used was an ATI Mini45 sensor with a *SI-580-20* calibration. The sensor measures forces accurately up to 580N in x- and y-direction, as well as up to 1160N in z-direction. It also measures torques in x-, y- and z-direction of up to 20Nm. All forces are reported at a resolution of 1/4N. Torques are measured at a resolution of 1/188Nm in x- and y-direction and at a resolution of 1/376Nm in z-direction (ATI Industrial Automation Manual 2016). There was also a smaller, more sensitive version of the sensor available but it was not used due to the risk of damaging the sensor with the rather high weight of the robot.

The sensor was placed inside a custom made foot and leg. Both parts were split into a top and a bottom part, which were connected only through the sensor. For the foot, the sensor was placed accurately below the center of mass of the leg as can be seen in Figures 5 and 6. For the leg, the sensor was placed exactly in the middle of the leg as shown in Figures 7 and 8.

4.1.5 Analysis of Forces

Figure 9 shows the torque of the knee servo motor, and the position of the motor as well as the force in z-direction captured by the ATI Mini45 f/t-sensor. Each peak of the blue line indicates a lift of the right leg and foot. On impact with the ground a negative peak can be seen in the force graph followed by a short oscillation due to flexibilities in the leg and the ground. The negative values for the force in z-direction are accountable to the mounting direction of the sensor inside the leg. On impact of the left foot, there is a noticeable reduction in force followed by a short double support phase before the pattern repeats. The duration of one step is 1.75 seconds as can be seen from the graph. Since the leg is angled during the walking motion, the total force acting on the leg is not equal to the force in z-direction, but to the combination of the forces of all axes. This sum is shown in Figure 10.

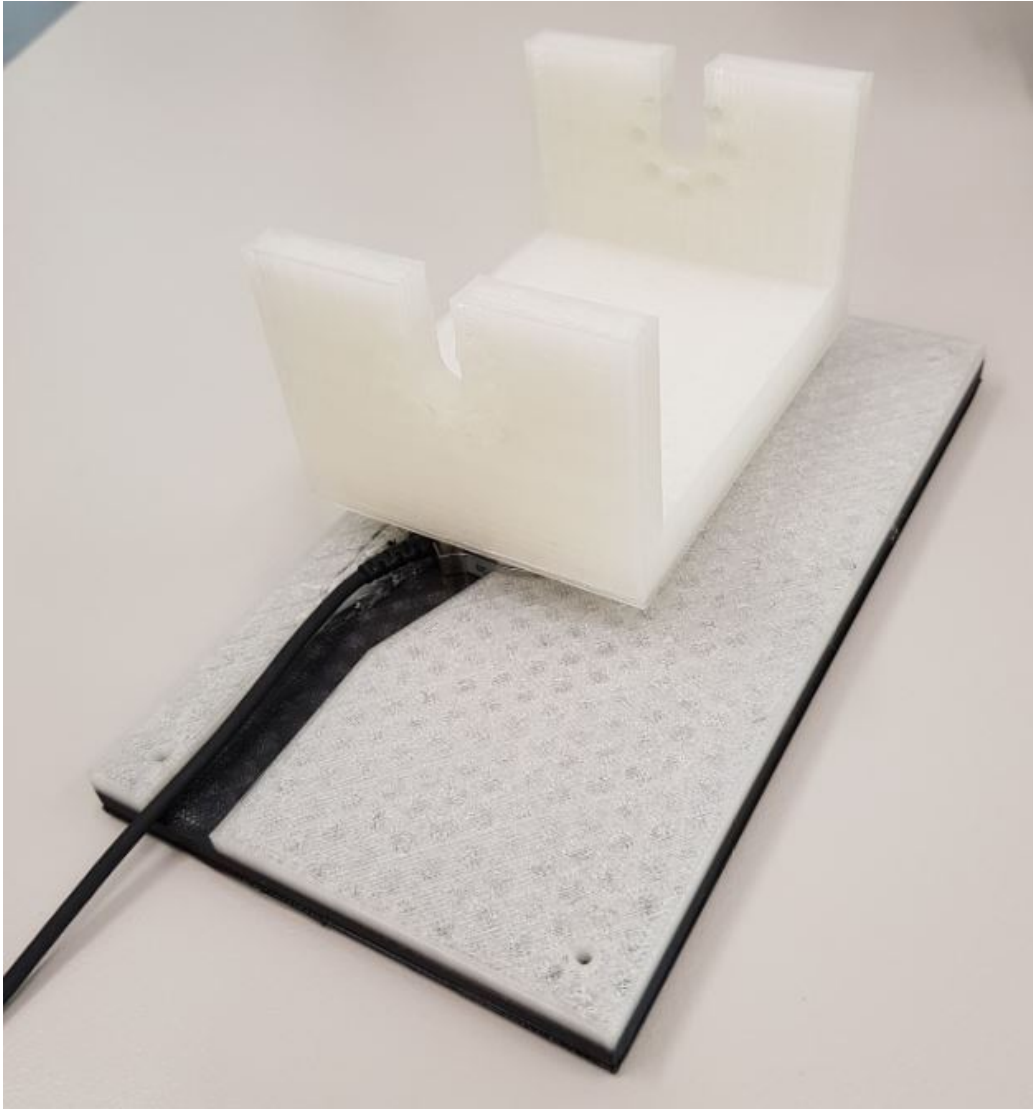


Figure 5: 3D-printed foot with a top and bottom part which are connected by an ATI Mini45 f/t-sensor

In order to incorporate the values into the FEA, I only used a subset of values, representing one step at certain equally spaced time stamps as can be seen in Table 1. For the foot, the graph in Figure 11 also quite clearly shows a repeating pattern for each step. The impact on the ground can be seen as a negative spike of the force in z-direction. As with the leg, the impact of the second foot reduces the force in z-direction significantly and transitions



Figure 6: 3D-printed foot with closer look at an ATI Mini45 f/t-sensor connecting the top and bottom part

into a short double support phase.

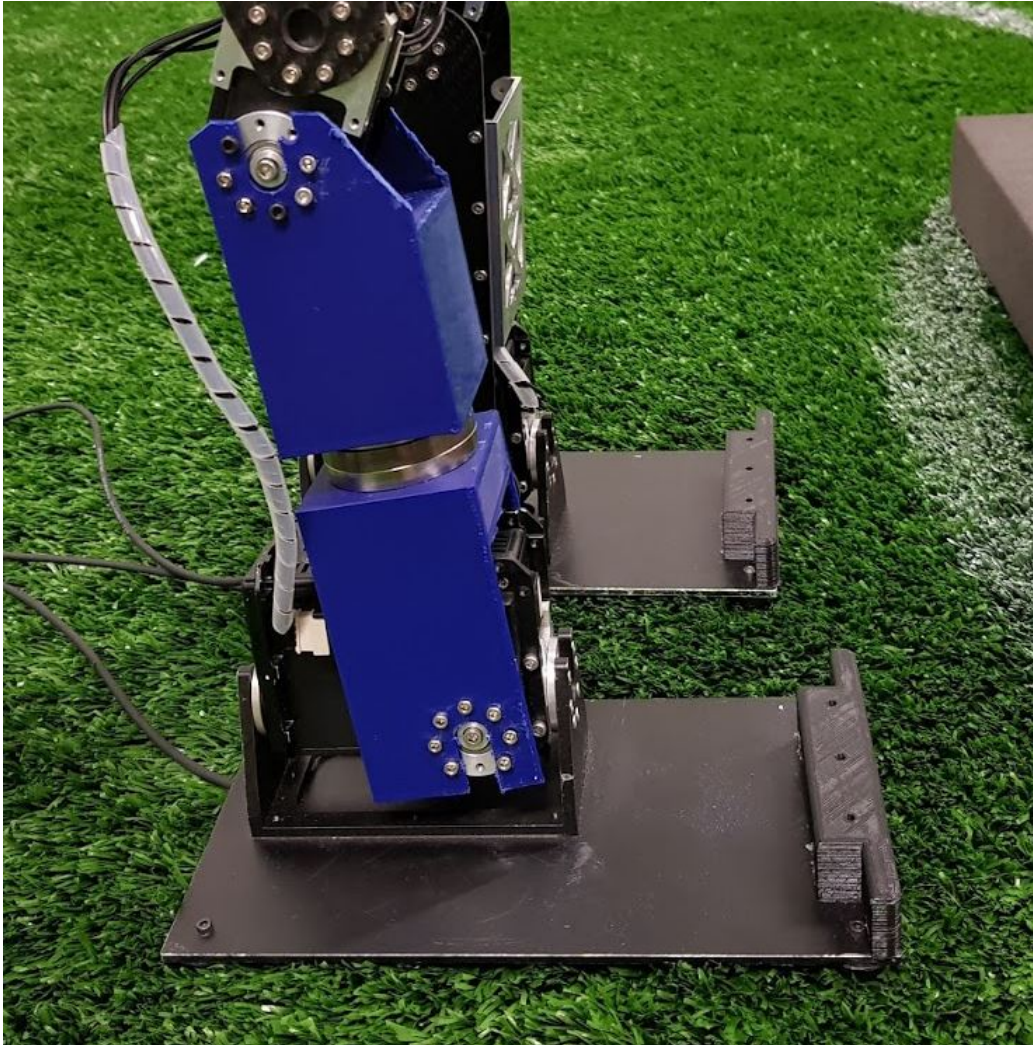


Figure 7: 3D-printed leg split in the middle with an ATI Mini45 f/t-sensor connecting the two parts

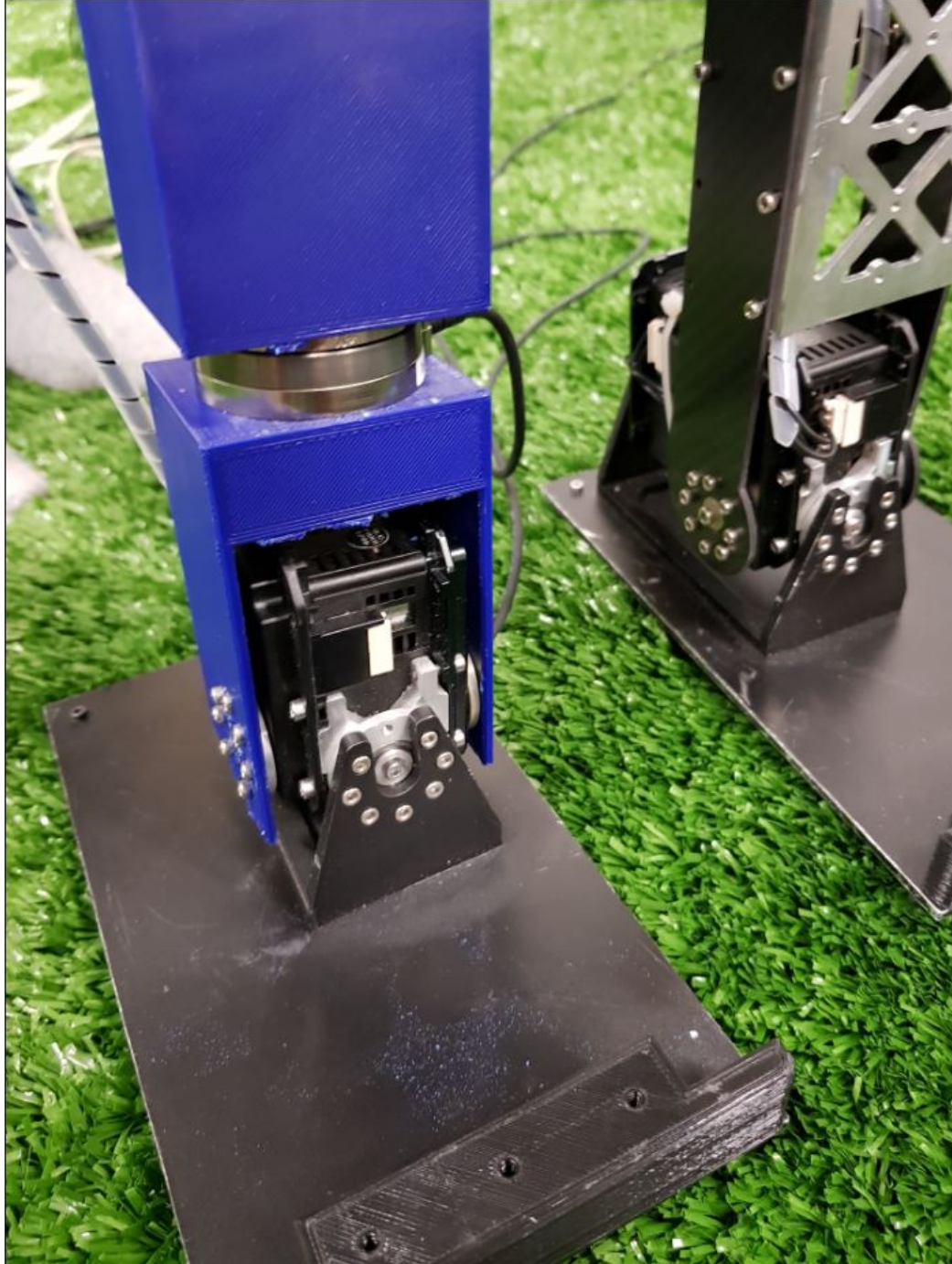


Figure 8: Front view of a 3D-printed leg split in the middle with an ATI Mini45 f/t-sensor connecting the two parts

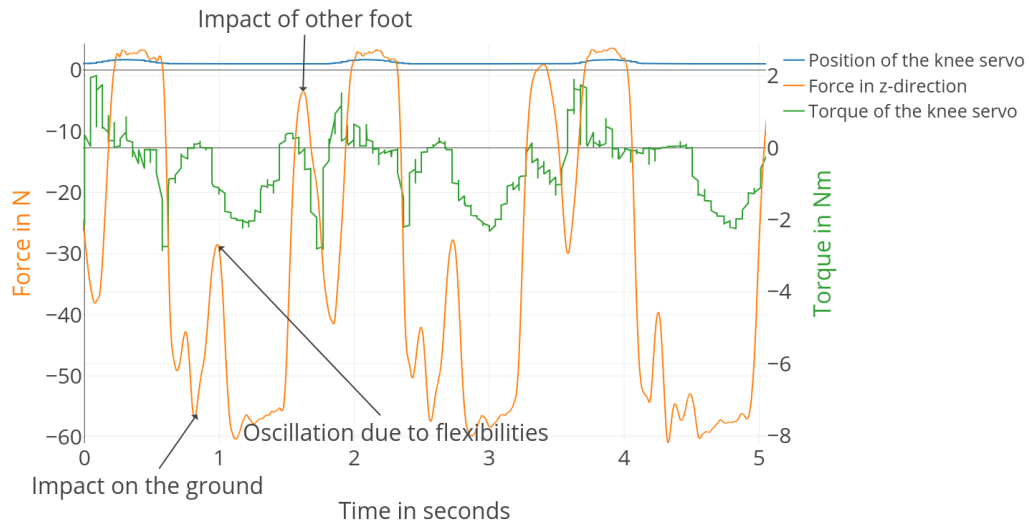


Figure 9: Graph showing the force and torque inside the knee of the robot over multiple steps with annotated events

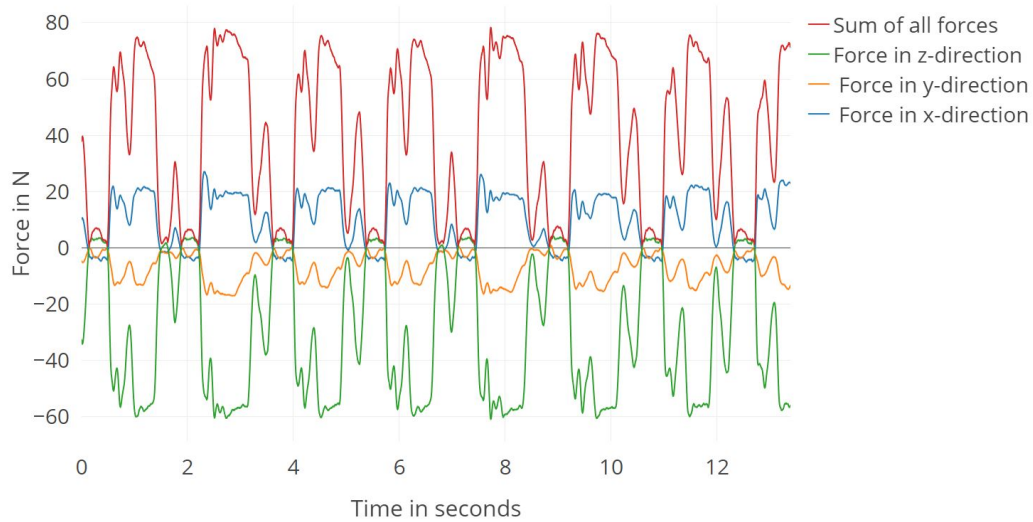


Figure 10: Graph showing the forces inside the knee of the robot over multiple steps with sum of all axes' forces

Time in seconds	Force in N			Torque in Nm		
	x	y	z	x	y	z
0.0	7.235	-4.291	-27.188	-0.379	-1.416	-0.015
0.1	12.420	-6.116	-37.435	-0.168	-1.381	0.108
0.2	0.798	-1.694	-5.808	0.038	-0.289	-0.158
0.3	-3.743	-2.800	3.118	-0.207	0.400	-0.166
0.4	-3.738	-3.197	2.90	-0.251	0.368	-0.182
0.5	-3.627	-0.860	1.830	-0.032	0.385	-0.173
0.6	-0.606	-1.442	-7.23	0.437	-0.220	0.033
0.7	19.559	-12.231	-48.732	0.67	-1.475	0.475
0.8	18.285	-12.827	-54.10	0.384	-1.68	0.653
0.9	14.606	-9.406	-45.468	-0.259	-1.562	0.034
1.0	8.483	-5.356	-29.133	-0.59	-0.884	-0.172
1.1	19.179	-12.787	-59.36	-1.254	-1.360	-0.205
1.2	20.000	-13.873	-56.39	-1.669	-1.211	-0.391
1.3	21.043	-11.927	-57.057	-1.847	-1.215	-0.68
1.4	20.210	-8.190	-55.813	-1.840	-1.326	-0.723
1.5	16.981	-7.481	-48.060	-1.761	-1.475	-0.939
1.6	0.105	-1.882	-4.739	-0.258	-0.086	-0.358
1.7	1.693	-1.888	-15.568	-0.337	-0.714	-0.215
1.8	6.432	-3.667	-26.481	-0.375	-1.183	0.134

Table 1: Force and torque inside the knee of the robot over 1.8 seconds with a resolution of 0.1s

Time in seconds	Force in N			Torque in Nm		
	x	y	z	x	y	z
0.0	0.128	-3.630	-7.883	1.000	-0.760	0.133
0.1	5.847	-6.420	-57.294	2.838	-1.241	0.358
0.2	3.909	-4.451	-50.304	2.455	-1.457	0.173
0.3	-0.856	-5.531	-47.825	2.380	-1.730	0.100
0.4	-1.367	-4.592	-47.749	2.002	-1.940	0.281
0.5	0.511	-2.442	-22.913	1.093	-1.335	0.225
0.6	0.306	-1.032	9.976	0.190	-0.259	0.101
0.7	-1.251	-0.442	9.415	0.121	-0.279	0.049
0.8	0.186	-0.460	-2.864	0.218	-0.677	-0.026
0.9	0.174	-1.617	3.894	0.381	-0.457	0.055
1.0	-0.291	-1.538	12.125	0.101	-0.179	0.069
1.1	0.620	-1.581	12.758	0.056	-0.169	0.084
1.2	0.256	-1.533	12.761	0.054	-0.161	0.083
1.3	-0.056	-1.643	12.496	0.049	-0.154	0.088
1.4	3.143	-3.654	-25.125	1.021	-0.701	0.209
1.5	8.094	-2.367	-26.779	0.729	-0.634	0.110
1.6	2.502	-2.824	-9.115	0.710	-0.776	0.117
1.7	0.240	-1.316	6.141	0.347	-0.398	0.105
1.8	0.302	-3.114	-0.844	0.782	-0.620	0.117
1.9	4.941	-6.484	-55.250	2.851	-1.982	0.329
2.0	1.594	-5.931	-46.836	2.471	-1.979	0.182

Table 2: Force and torque inside the foot of the robot over 1.8 seconds with a resolution of 0.1s

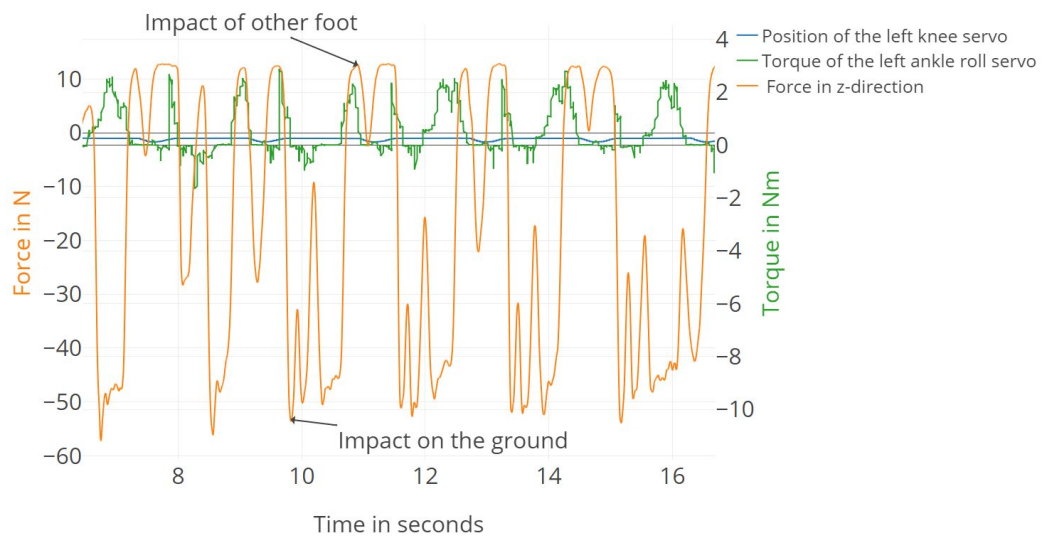


Figure 11: Graph showing the force and torque inside the left foot of the robot over multiple steps with annotated events

4.2 Tools Used

In this section, the tools that were used to create and optimize the parts of the robot are described.

4.2.1 ANSYS Workbench Suite

Since FEA and topology optimization tasks are practically unsolvable by hand, the calculations as well as the modellations of the parts have been produced using third-party software. There is a variety of software solutions available to produce 3D-models, perform FEA as well as carry out topology optimization tasks. Most of these tools are commercially licensed but often offer a free downgraded version for educational use.

The software solution used in the process of creating the parts for this thesis as well as in any of the analyses and optimization tasks, is the ANSYS Workbench suite. The suite offers various software solutions for many applications, such as fluid dynamics, static structural analyses and thermodynamic simulations. All of these solutions are easily combinable due to the modular work-space system offered by the Workbench suite shown in Figure 13. The main reason for choosing the ANSYS Workbench simulation suite was the ease with which each software component can be operated paired, with the extensive functionality offered by the suite.

In the process of optimizing the topology of a robotic part, three tools including the Workbench are used. Besides the Workbench, a Computer Assisted Design (CAD) tool called *SpaceClaim* as well as a mathematical solver program called *Mechanical* are utilized to complete the process of optimizing a part. The typical workflow with the ANSYS Workbench starts with creating a static structural analysis module in the Workbench itself. Then, material properties for the parts need to be defined. In my case, material properties as researched by Torres et al., 2015 were used as shown in Figure 12. The module is then equipped with a 3D-model of the part, which itself can either be imported from various formats or directly designed within *SpaceClaim*. When designing a part in *SpaceClaim*, I started off by sketching the bottom face of the part on a plane. This sketch was then pulled to the

1	Property	Value	Unit
2	Material Field Variables	Table	
3	Density	1,24	g cm ⁻³
4	Isotropic Elasticity		
5	Derive from	Young's Modulus and Poisson's Ratio	
6	Young's Modulus	3500	MPa
7	Poisson's Ratio	0,36	
8	Bulk Modulus	4,1667E+09	Pa
9	Shear Modulus	1,2868E+09	Pa

Figure 12: ANSYS Workbench table showing the material properties for PLA

proper height, creating a 3D-object. Holes, curvatures and other details were then sketched on the proper faces of the part and extruded in- or outwards to create the desired surface. The finished part was automatically imported by the ANSYS Workbench into the right slot. After the design step the model was then loaded into *Mechanical*, in order to perform analysis on it. The first step of analyzing was to mesh the part. The initial meshing was performed rather quickly but needed some refinement to fit the provided model more properly. After the mesh for the part was obtained, load and support conditions were defined for the part. All of the offered condition-types can be applied to one or multiple faces of the part. After the constraints have been set, the actual analysis could be triggered. The finished structural analysis is automatically imported into the proper workbench-slot as well.

In the next step, a topology optimization module was added to the workbench. The solution obtained by the static structural module is injected into the topology optimization module. This way, all already defined constraints and settings are reapplied. After defining design and exclusion regions for the solver, the topology optimization task can be carried out and produces a stereolithography (STL)-model. The obtained stl file is then reimported into a static structural module to fix the STL-model and smooth it's surface.

4.2.2 Slic3r

After a smoothed STL-file has been obtained through the optimization process, the model needs to be prepared for 3D-printing. This is done by using

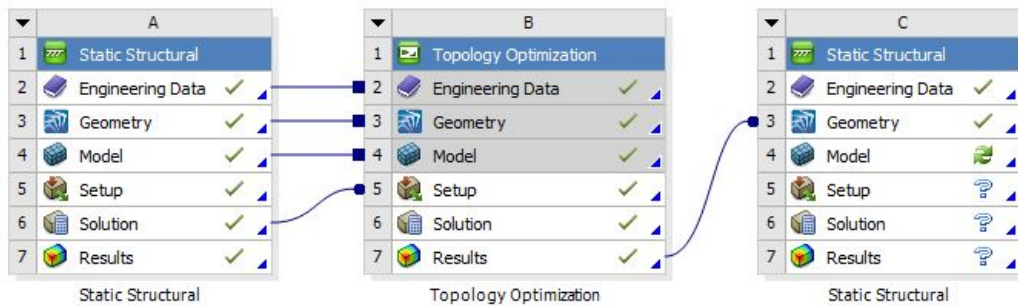


Figure 13: Workflow elements as seen in the ANSYS Workbench showing links between different steps of the optimization process

a slicer. A slicer divides the STL-model into thin slices called layers, which are printed one after another. Additionally, the slicer translates the instructions about the layers, the speed at which the layers should be printed as well as miscellaneous information such as the type and percentage of infill and whether or not support material should be generated, into control commands for the printer. These control commands are written in a language called g-code. A software called *slic3r* was used to perform these steps.

4.2.3 Prusa i3

After a model has been prepared for 3D-printing, a printer is needed in order to produce the part. For the production of the optimized parts, I was able to choose between 4 different printer-types. Two of them were FDM-printers, one using PLA and the other using ABS. The third was a SLA-printer and the fourth a multijet-printer. I decided to use the Prusa i3 FDM-printer using a PLA filament. It had a large enough print bed of about 20cm by 20cm and was relatively simple to repair and to extend. Additionally, the cost of parts produced on the Prusa i3 is significantly lower than on multijet or SLA-printers simply due to the cost of the used material. Time-wise the FDM-printer turned out to be the fastest as well. While the SLA and multijet printer gave estimations of around 24 hours, the Prusa i3 completed the same print in approximately seven hours.

4.3 Topology Optimization of the Lower Right Leg

The process of optimizing the lower right leg of the robot mainly consists of three phases. The first phase involves modelling the leg with its space, load and support constraints as well as optimization objectives and parameters. In the second phase the optimization software optimizes the model based on the earlier defined constraints and settings. In the final phase, the results are evaluated and it is decided whether to manufacture the part or to tweak optimization parameters and restart the optimization.

4.3.1 Modeling the Leg

In order to give the optimizer the highest possible amount of material to work with, the part to be optimized is simplified to only meet all sizing constraints. For the lower right leg, these constraints are the height, width and depth, as well as cutouts for the motors and cylindrical cutouts for the mounting plate of the motors. Also the shape of the top and bottom end needs to meet some collision constraints. The height, width and depth can be measured simply by measuring the 3D-model of the leg in *SpaceClaim*. This gives us a height of 205mm, a width of 56mm and a depth of 51mm. We start out by creating a cuboid with these measurements. The holes for mounting the motors are placed on the sides of the cuboid. The center hole is 11mm in diameter and is surrounded by 8 smaller holes for M2.5-screws. The center hole has a distance of 17.7mm to the top or bottom border of the cuboid. For the leg to not collide with the foot or the upper leg, it is rounded on the top and bottom end.

Figure 14 shows a side view of the lower leg with the mounting holes and curvature on the top and bottom end. To be able to mount the servo motor inside the leg, cutouts are needed. The servo-motor used in the robot, the *Dynamixel MX-106t*, is 42mm deep 46mm wide 60mm high. The cutouts for the motor need to be a bit deeper to ensure that the motor can turn freely inside the leg. In order to determine how much material needs to be removed, the motors are imported as 3D-models into *SpaceClaim* and the leg is rotated to show possible collision points as shown in Figure 16. The

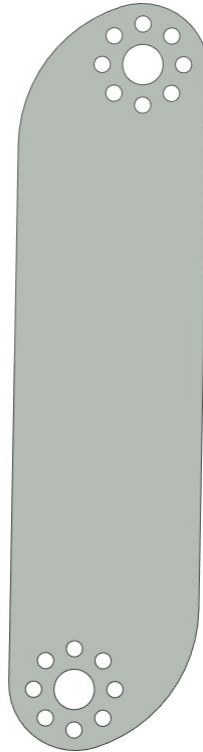


Figure 14: Side view of the lower right leg with mounting holes for a servo motor

cutouts are then adjusted to account for those constraints. After freeing the space for the servos, the leg resembles an h-shape and uses the maximum amount of material while still meeting all previously mentioned constraints as shown in Figure 15.

4.3.2 Simulating the Leg under Load

In order to accurately simulate the behaviour of the leg under load, the leg is imported into *Mechanical* with a 3D-model of the foot attached to the bottom axis. The motor-axes are simplified with cylinders. Figure 17 shows the back view of the setup with the leg tilted forward to match the pose of the real robot in Figure 18. With the data reported by the sensor, loads can be defined acting on specific faces of the leg. I defined a force that acts

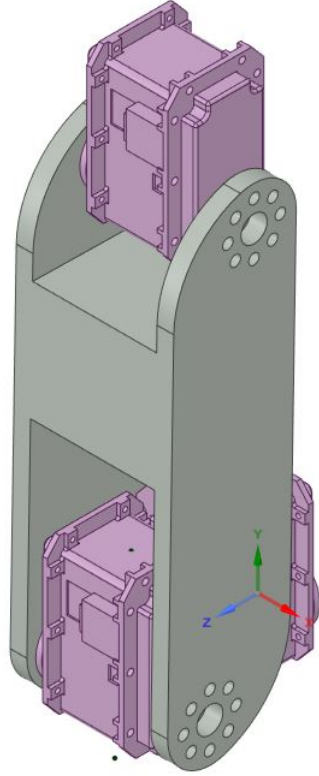


Figure 15: Front view of the leg with motor-models to verify cutout dimensions

on the upper axis. The simulation was divided into 18 simulation steps, each with a length of 0.1s. This matches the recordings of the sensor. The values were directly inserted into the simulation as shown in Figure 21. The torques measured by the sensor are defined to act on the center faces of the leg as shown in Figure 20. The whole system is defined to be supported on the bottom of the foot. The support points are the four contact points for the studs that will be installed after the print has finished. After running the simulation we obtain a detailed distribution of the stress deformation that occurred in the material during the simulation in Figure 23. This will be our foundation to determine, which sections of the part can be removed safely while still maintaining great enough stability in terms of the simulated loads.

The stress distribution model in Figure 23 clearly shows a large portion of

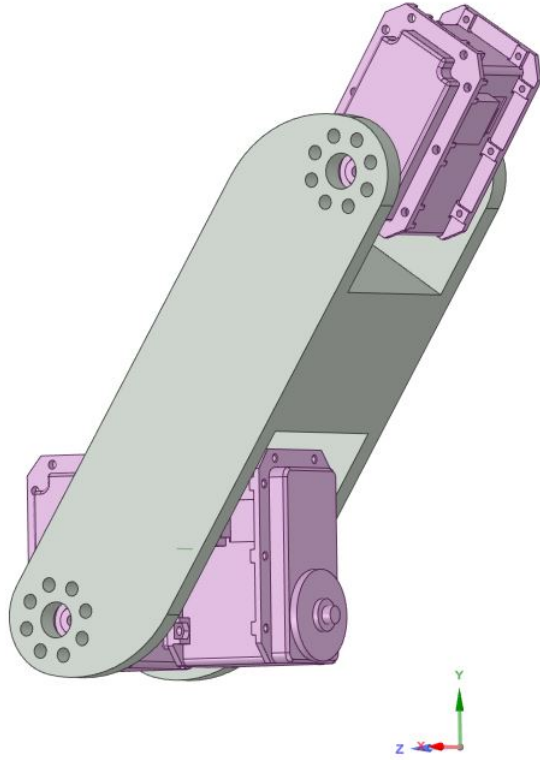


Figure 16: Rotated leg to check for possible collision with the servo motors

the stress occurring in and around the lower joint. The deformation shown by Figure 24 on the other hand, shows the most deformation happening on the top part of the leg.

4.3.3 Optimizing the Topology of the Leg

With the data obtained in the design and simulation step, we are now able to optimize the topology of the part. In order for the finished part to meet certain structural constraints, I defined design- and exclusion-regions. The exclusion-regions will remain untouched by the optimization while it will remove material from the design-regions. Since the motors need to be mounted using the earlier defined mounting holes, these are defined as the only exclusion-regions as shown in Figure 25. Besides the design- and exclusion-regions, we define some manufacturing and optimization constraints

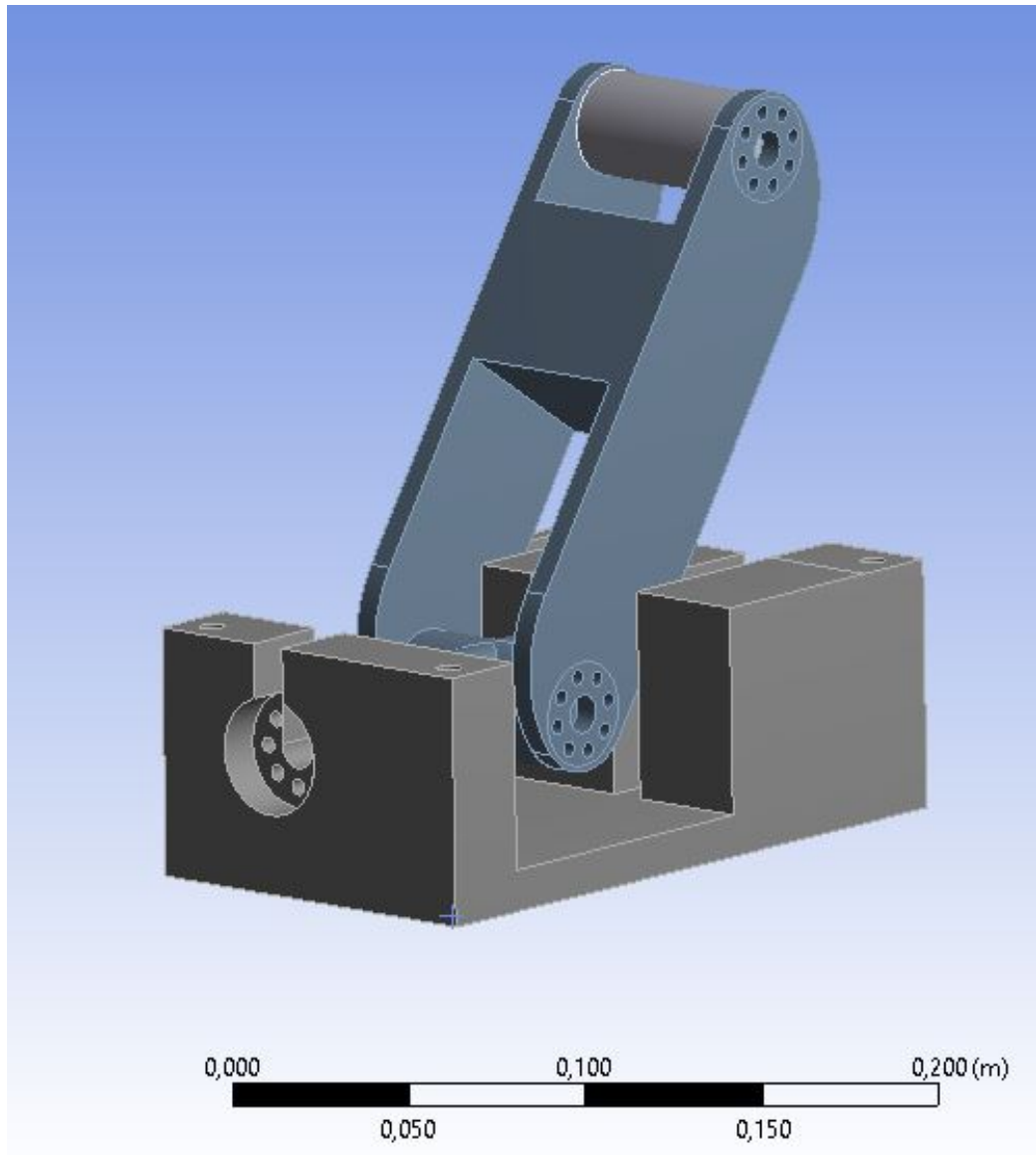


Figure 17: Leg attached to a 3d-model of the foot with simplified motor-axes

as well. The target for the optimization is set to retain at most 30% of the initial mass. In order to be able to print the optimized part, the minimum feature size is set to 1mm. With these constraints the optimization module of ANSYS returns the optimized topology as shown in Figure 26.

Though the part is now optimized based on the defined constraints, the structure of the returned faceted body is very coarse and needs post pro-



Figure 18: Walk ready pose of the Wolfgang robot

cessing. The post processing involves multiple actions. The first action is to fix the geometry of the STL-file. This can be done automatically by *SpaceClaim*. The auto-fix algorithm removes overlapping triangles, closes holes and fixes gaps in the structure. Completely disconnected facets, however, need to be connected manually to the faceted body or removed entirely. Figure 27 shows small disconnected facets that will be removed since they don't provide any structural improvements. After the part has been geometrically

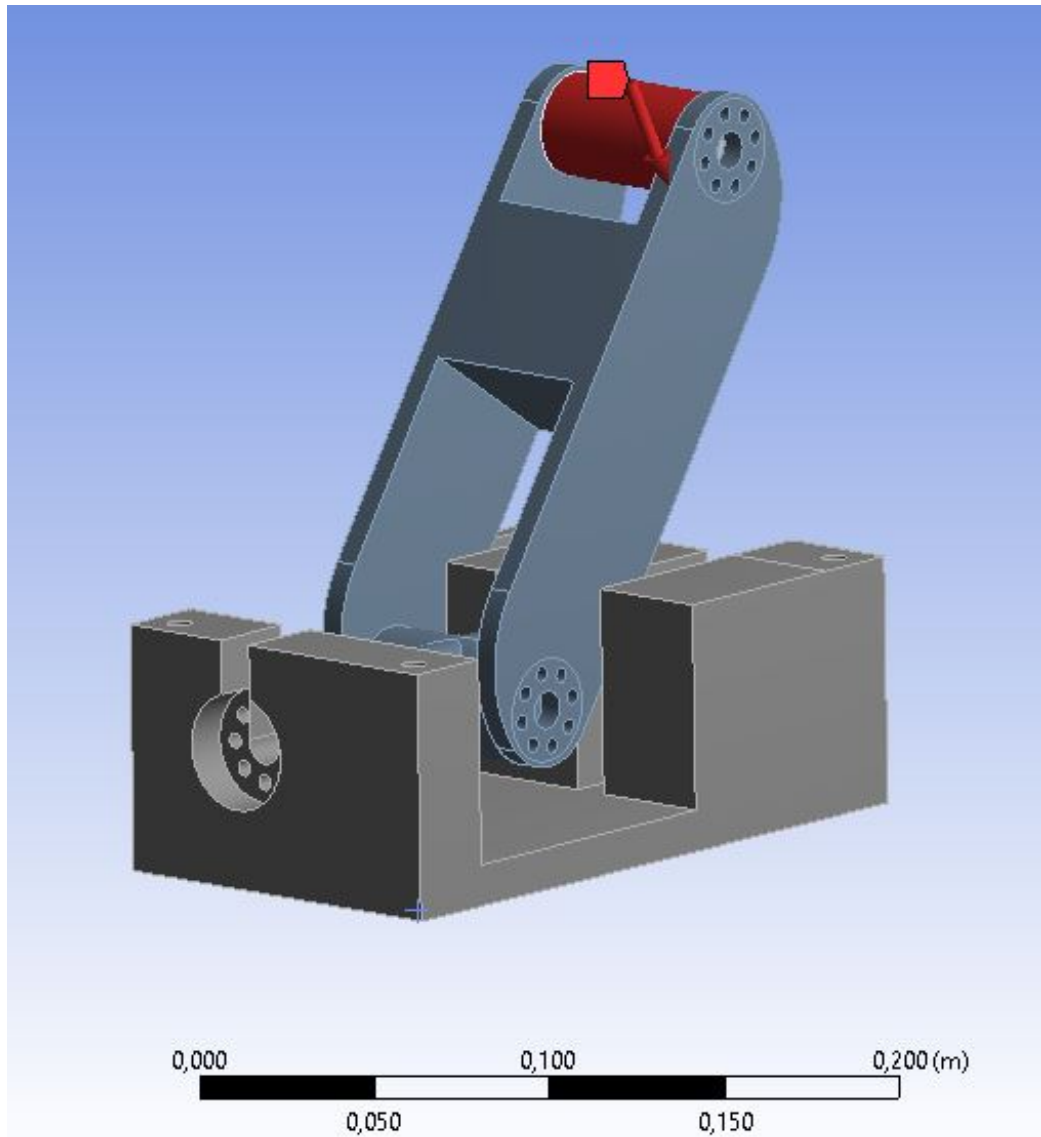


Figure 19: Back view of the modeled leg with faces selected for the forces in red

corrected, important geometric features can be added back to the part so that the smoothing later on does not interfere with critical elements such as mounting holes. Figure 28 shows important features of the original model in blue. The last step of the post processing phase is the smoothing of the part. This fixes very coarse approximations of the surface in areas where it is preferable to have a rather smooth surface e.g. around the mounting

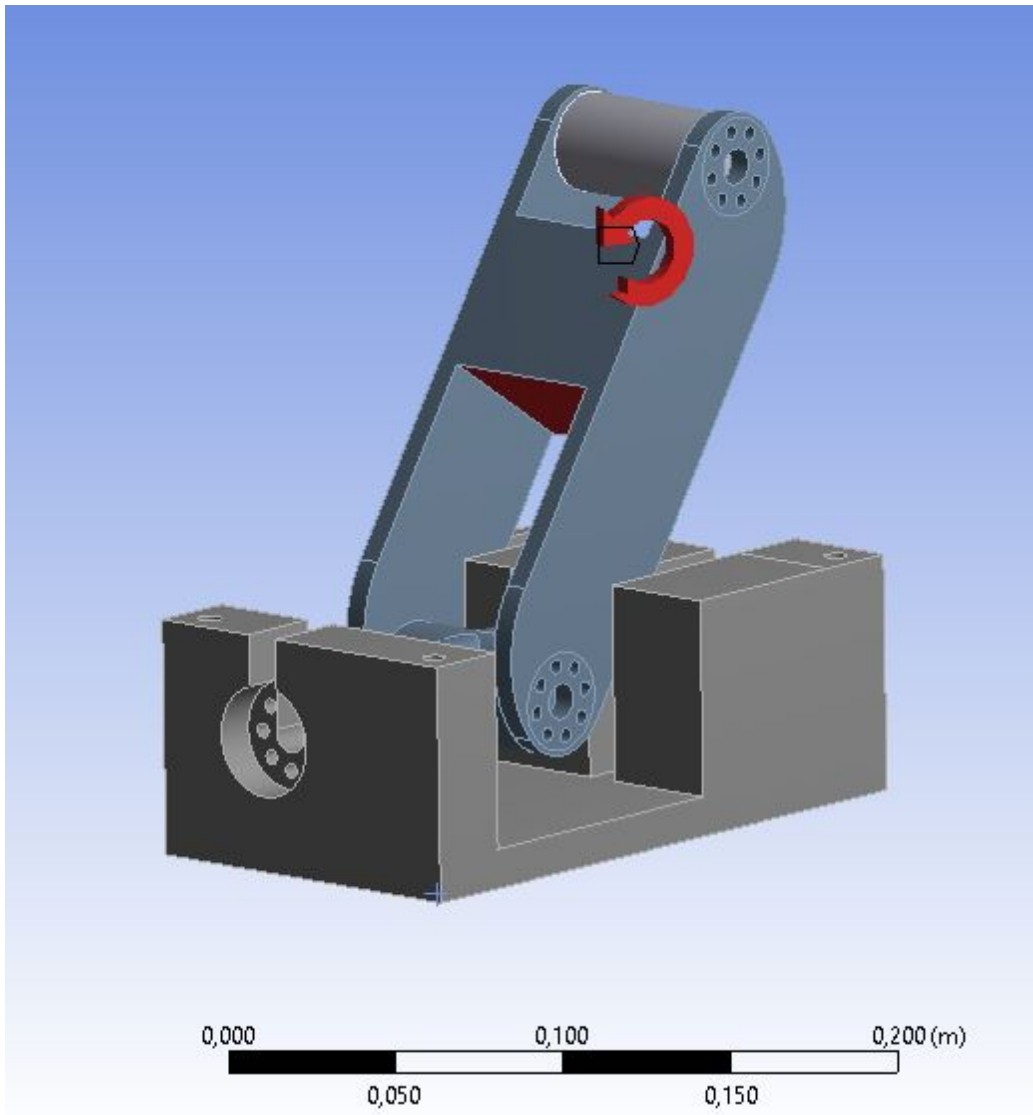


Figure 20: Back view of the modeled leg with faces selected for the torque in red

holes. The smoothing is adaptive so that it can be very fine in important areas while opting for a faster, more coarse surface in less complex areas. Figure 29 shows the finished smoothed surface of the lower leg and Figure 38 shows the leg connected to the modeled foot and motors. The finished smoothed part can now be manufactured using any type of AM. In order for the robot to walk properly, symmetry is of advantage so that the right leg

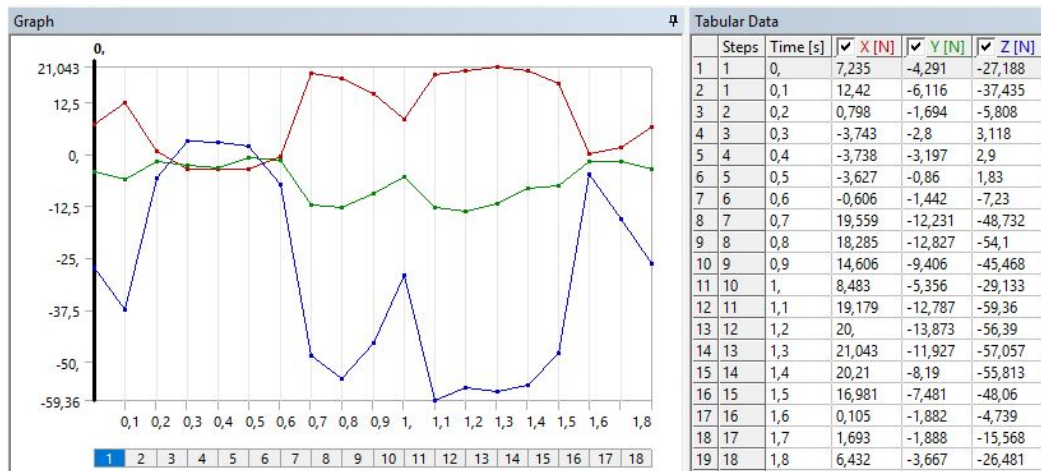


Figure 21: Forces defined to be acting on the top axis of the modeled leg

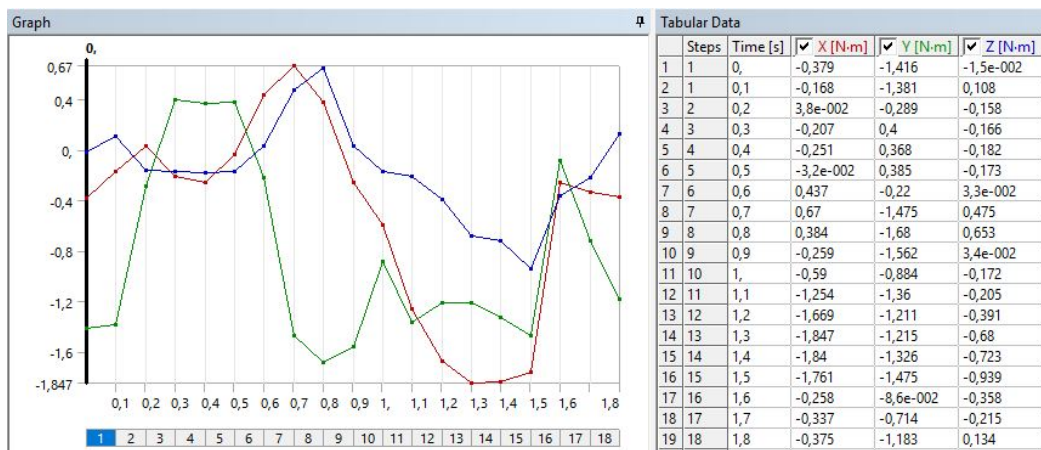


Figure 22: Torques defined to be acting on the center of the modeled leg

can be produced by simply mirroring the left leg.

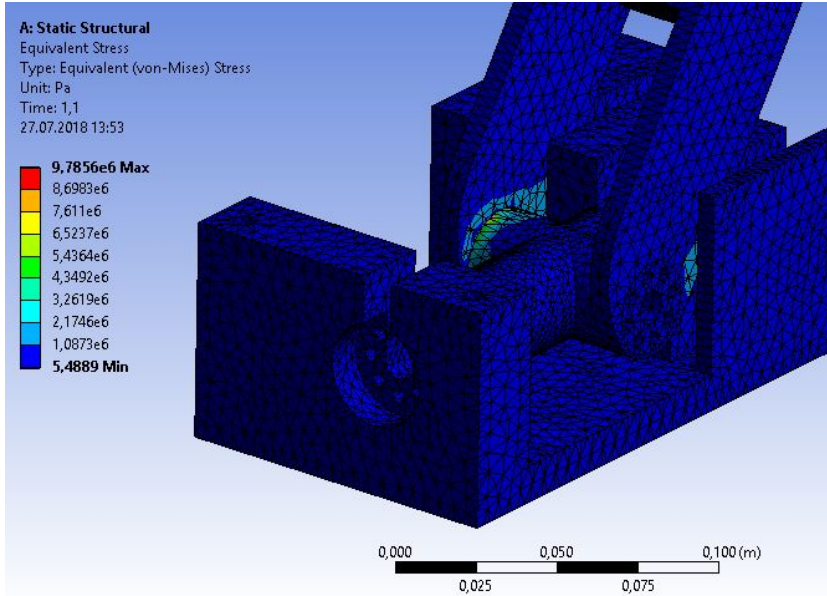


Figure 23: Distribution of stress in the material of the leg

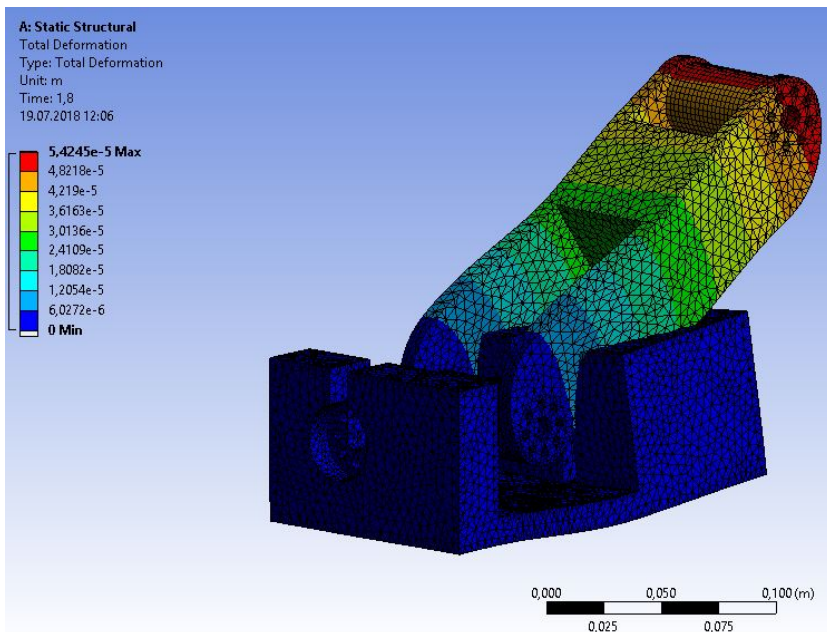


Figure 24: Distribution of deformation in the material of the leg

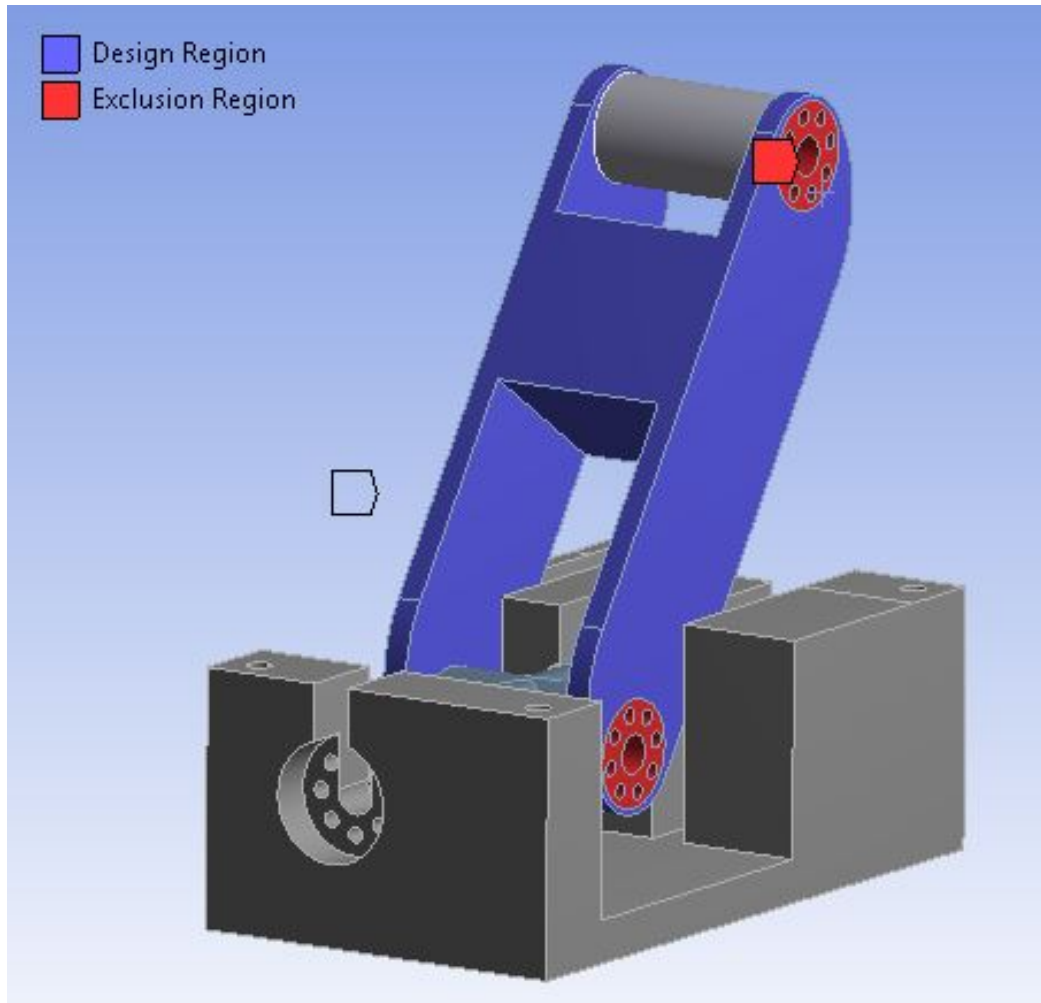


Figure 25: Back view of the leg showing design-regions in blue and exclusion-regions in red

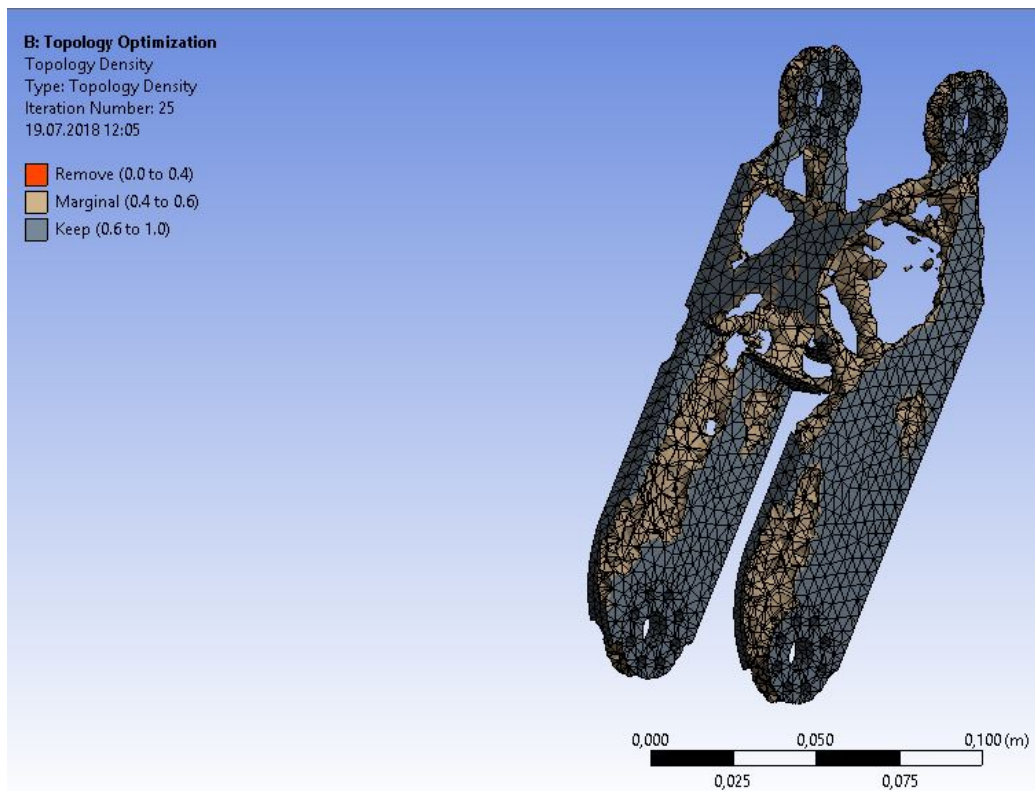


Figure 26: Raw response of the topology optimization of the lower leg

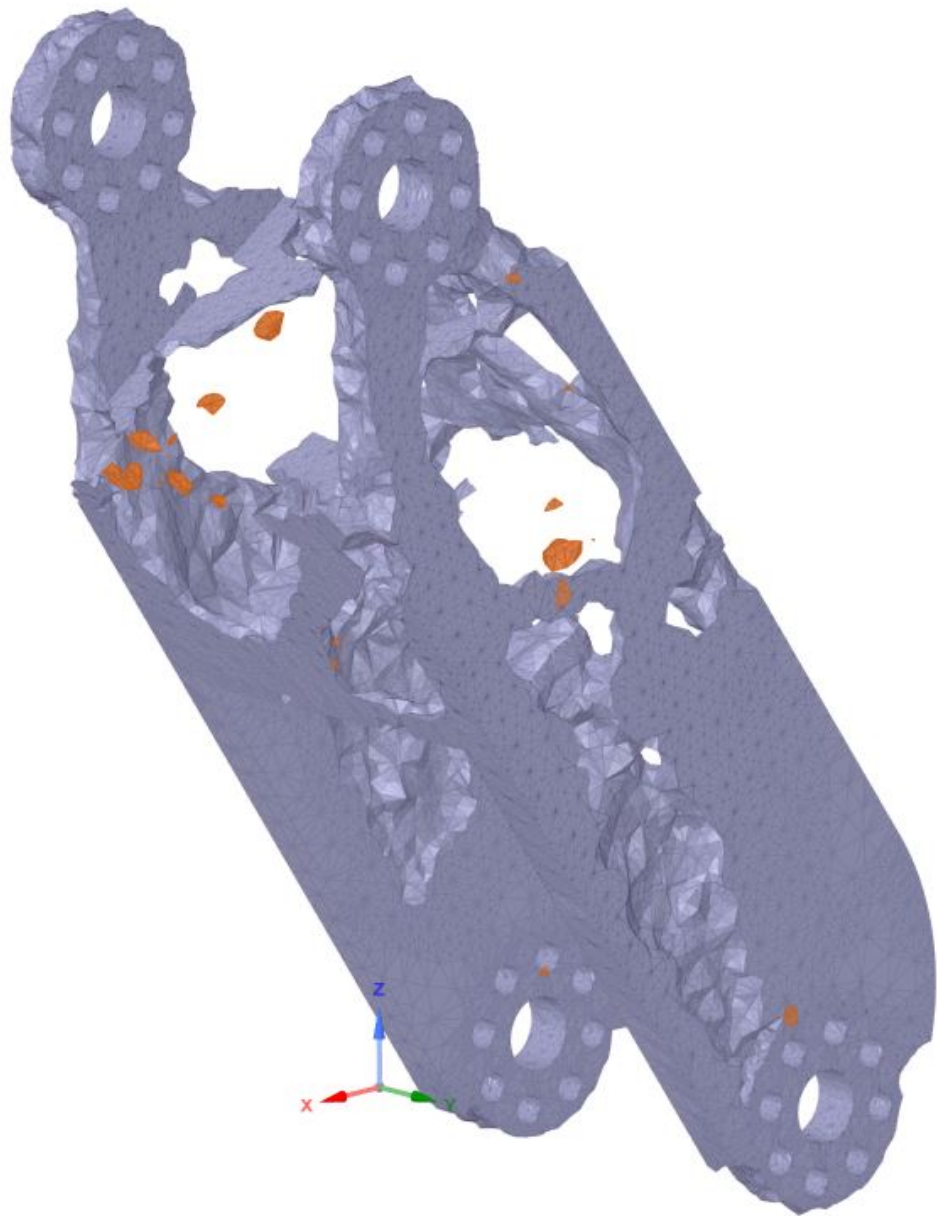


Figure 27: Optimized topology of the leg showing small disconnected facets highlighted in orange

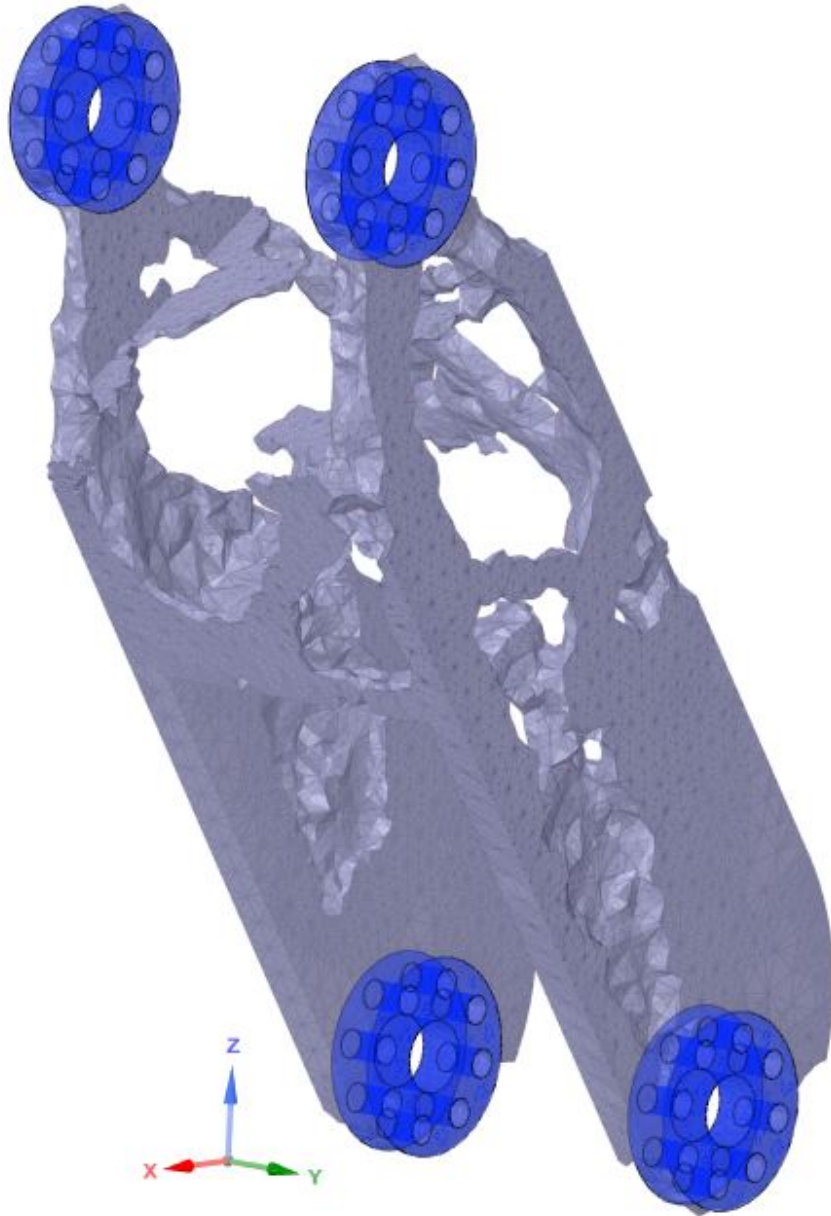


Figure 28: Optimized topology with important features to retain highlighted in blue

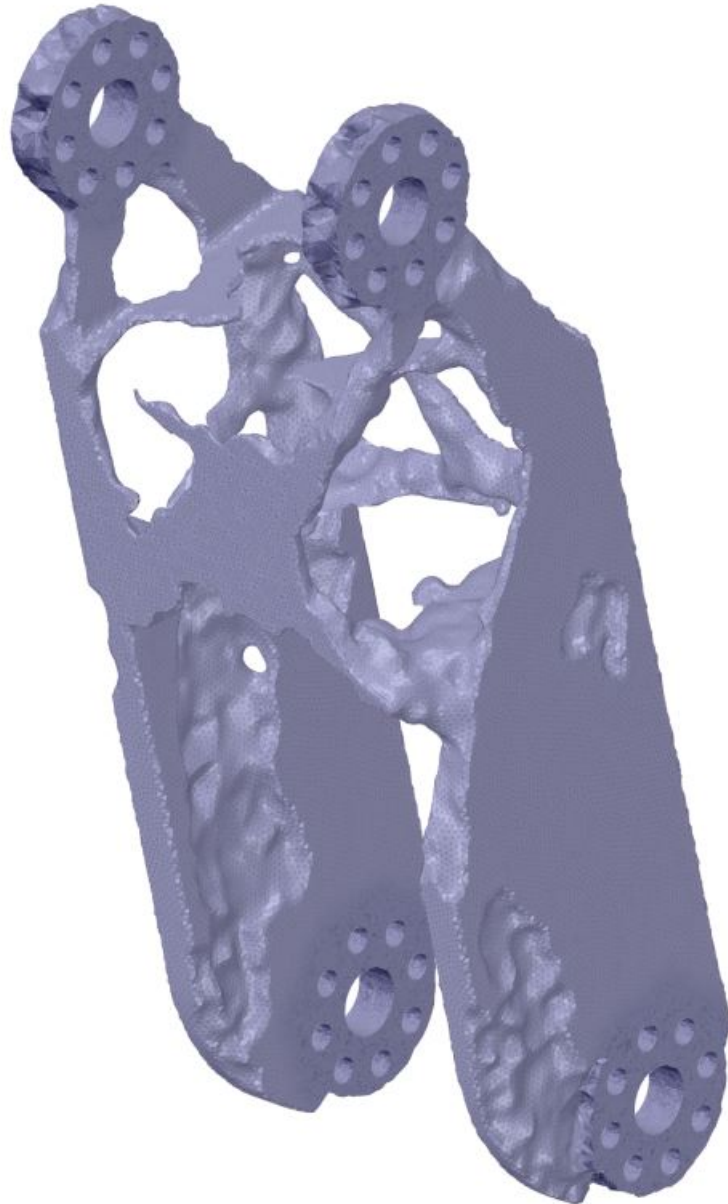


Figure 29: Optimized leg after smoothing

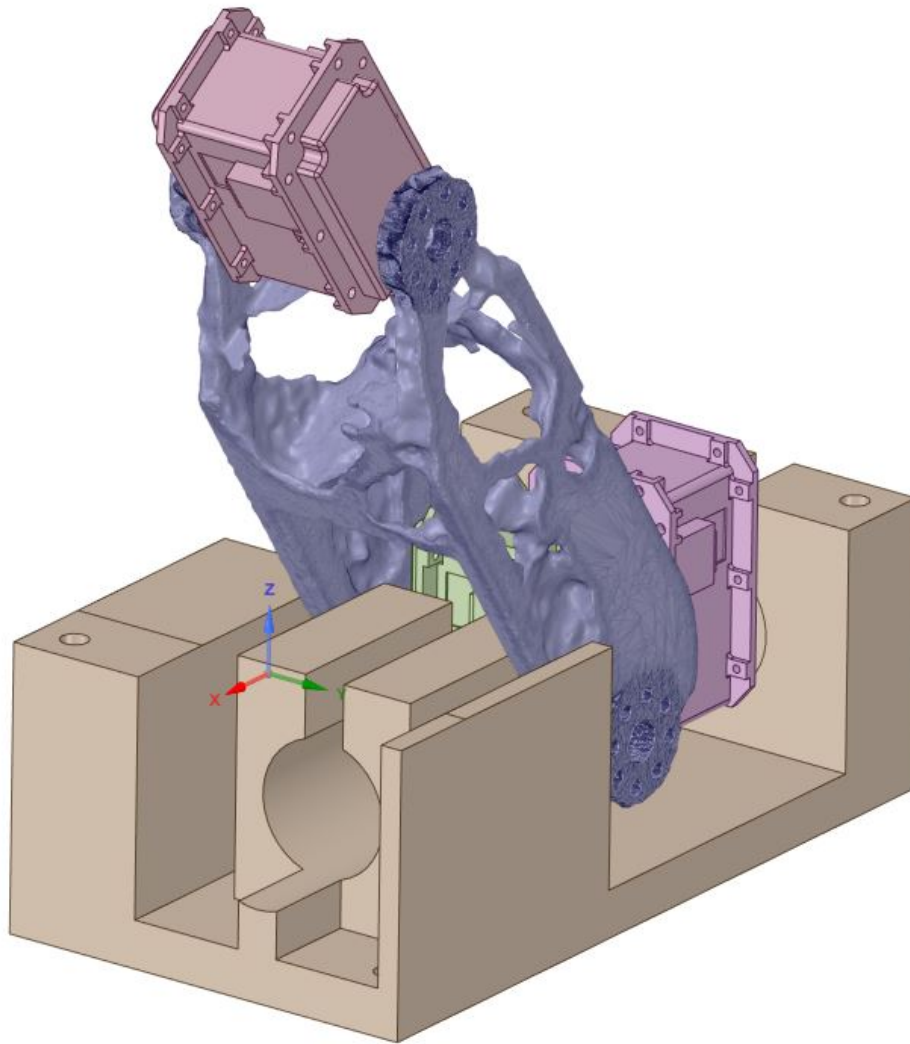


Figure 30: Front view of the optimized lower leg with foot and motors

Since the optimization searches for a material distribution to ensure maximum stiffness, given the mass constraint I defined, the leg retained most of its material at the lower end. This is the area in which most of the stress occurs. The top part experienced less stress and is therefore optimized significantly more than the lower part, resulting in the shown structure. The center block of the original 3D-model was removed almost entirely. Only thin connections between the left and right side remained.

4.4 Topology Optimization of the Foot

Analogously to the steps presented before, the left foot of the robot was optimized, as well. The foot is modeled as a block with a central cutout for two *Dynamixel MX-106* servos. Mounting interfaces are placed 4cm away from the bottom of the model along the longer axis of the foot. The thickness of the mounting interfaces is set to be 1cm and a circular area is defined, in order to later be specified as an exclusion region. On the bottom face of the block, four circular shapes are defined where studs are installed for the foot to have better contact with the ground and not bounce off of the grassy field. For the screws that will later hold the studs, four deep cylinders are defined to allow for the screws to sink completely into the finished part. The actual screw hole is placed at the bottom of the cylinders with a depth of 10mm. Since the servo motors of the robot have to slide into the foot from the top, a gap from the top of the foot to the center of the mounting face is defined. Figure 31 and 32 show the described model. Since the leg needs to be able to tilt forward for walking and standing up, a cutout is incorporated into the design of the foot. Figure 33 shows a possible collision with the foot avoided due to the cutouts.

As for the leg, the loads which act on the foot are defined on specific faces of the model and act over a time of 1.8s with 0.1s per time step. The loads and torques are directly taken from the values in Table 2 as shown in Figure The forces and torques are defined to act on the motor axis in x- and y-direction. Figure 34 and 35 show the deformation and stress inside the foot calculated by the FEA. For the optimization process, the mounting faces and

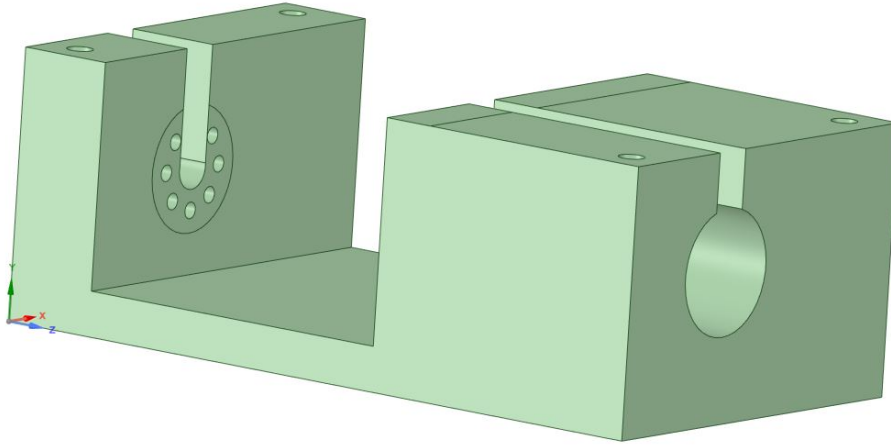


Figure 31: 3D-model of the foot designed to use the maximum amount of space available

the stud connections are defined as exclusion regions as can be seen in Figure 36. The settings for the optimization task itself were kept consistent with those for the leg. I defined a mass retention of 30% as well as a minimal feature size of 1mm.

The returned topology shown in Figure 37 needs to be geometrically repaired and smoothed. The finished part with the optimized lower leg and the optimized foot can be seen in Figure 38.

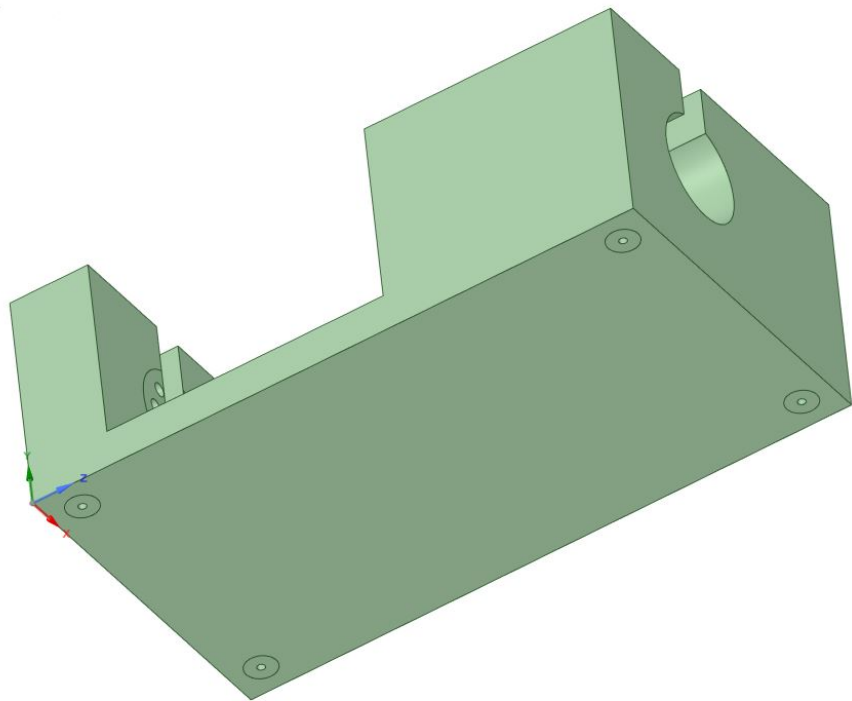


Figure 32: Bottom view of a 3D-model of the foot designed to use the maximum amount of space available

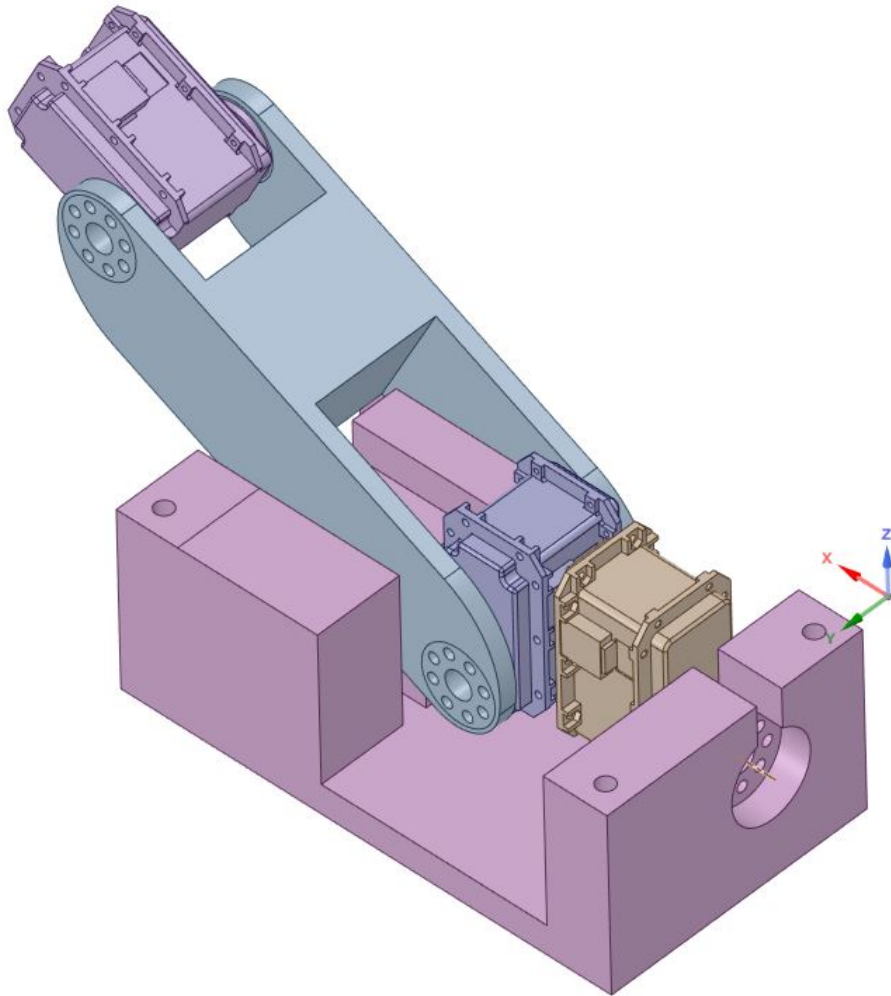


Figure 33: Model of the foot with cutouts and forward tilted leg to show possible collisions

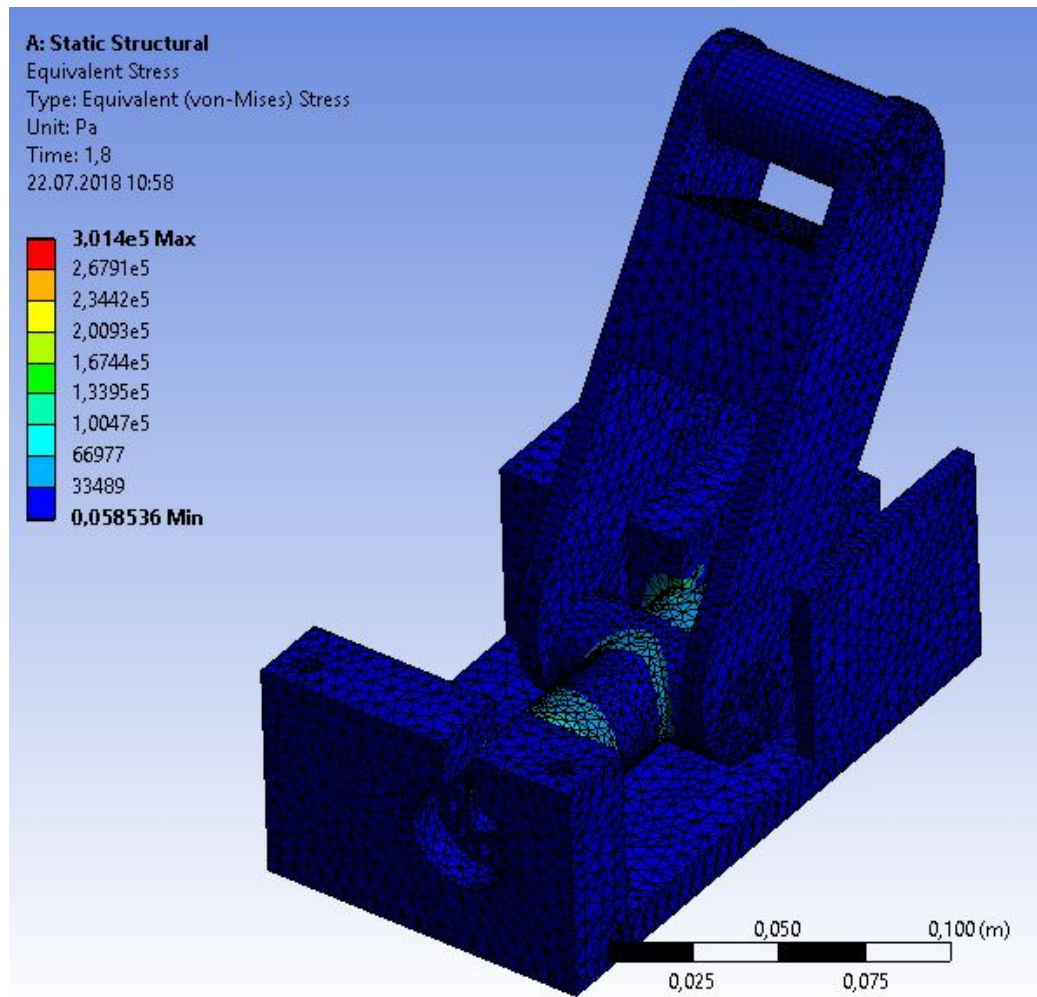


Figure 34: Distribution of stress inside the foot of the robot

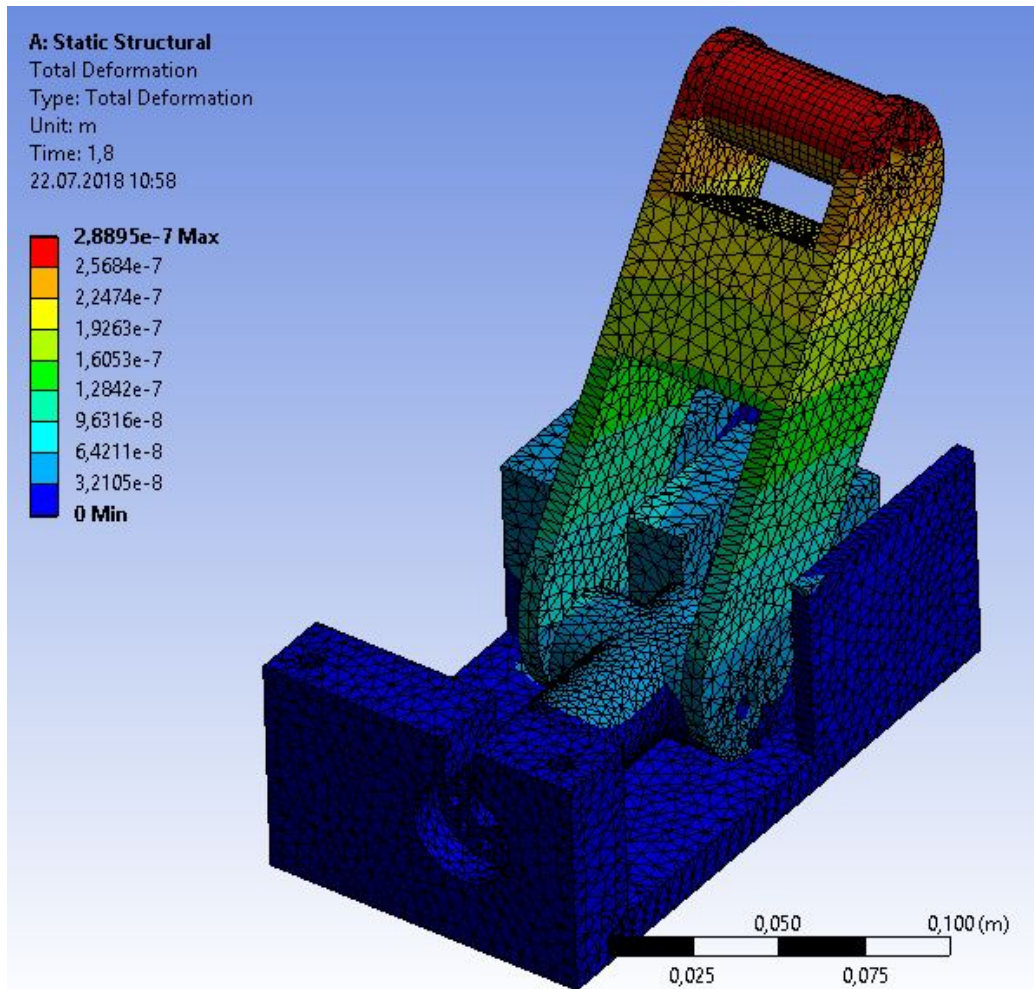


Figure 35: Distribution of deformation inside the foot of the robot

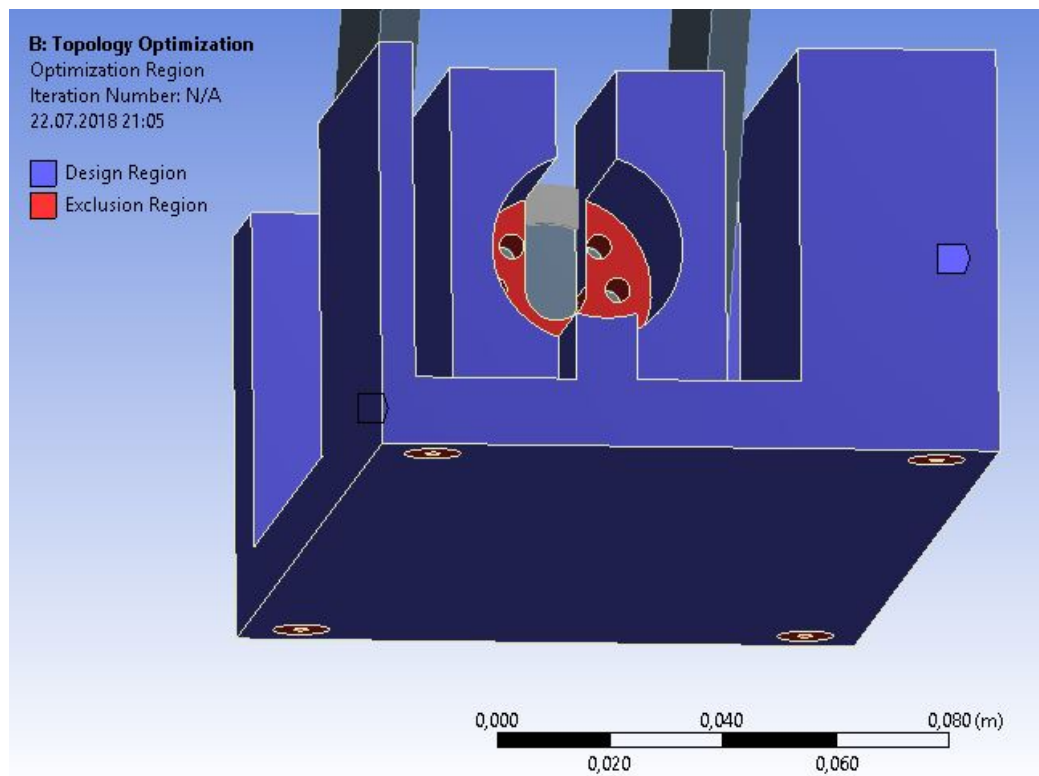


Figure 36: Design regions in blue and exclusion regions in red, defined for the foot for the topology optimization process

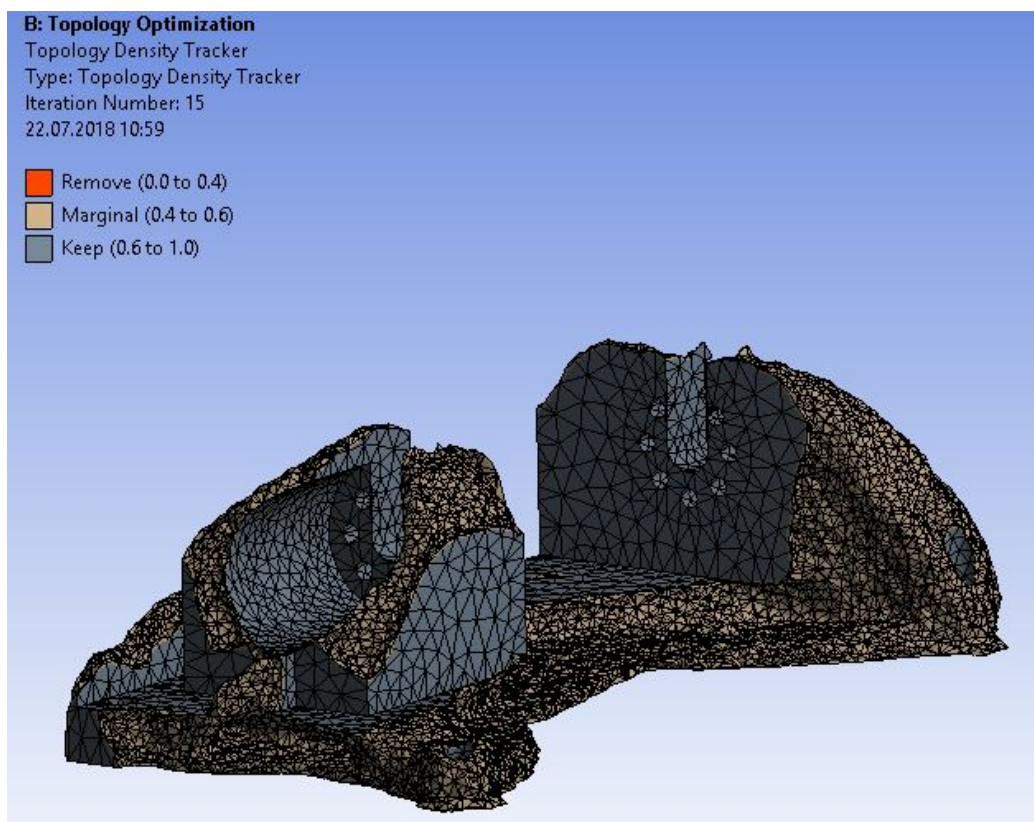


Figure 37: Raw result of the optimization for the foot

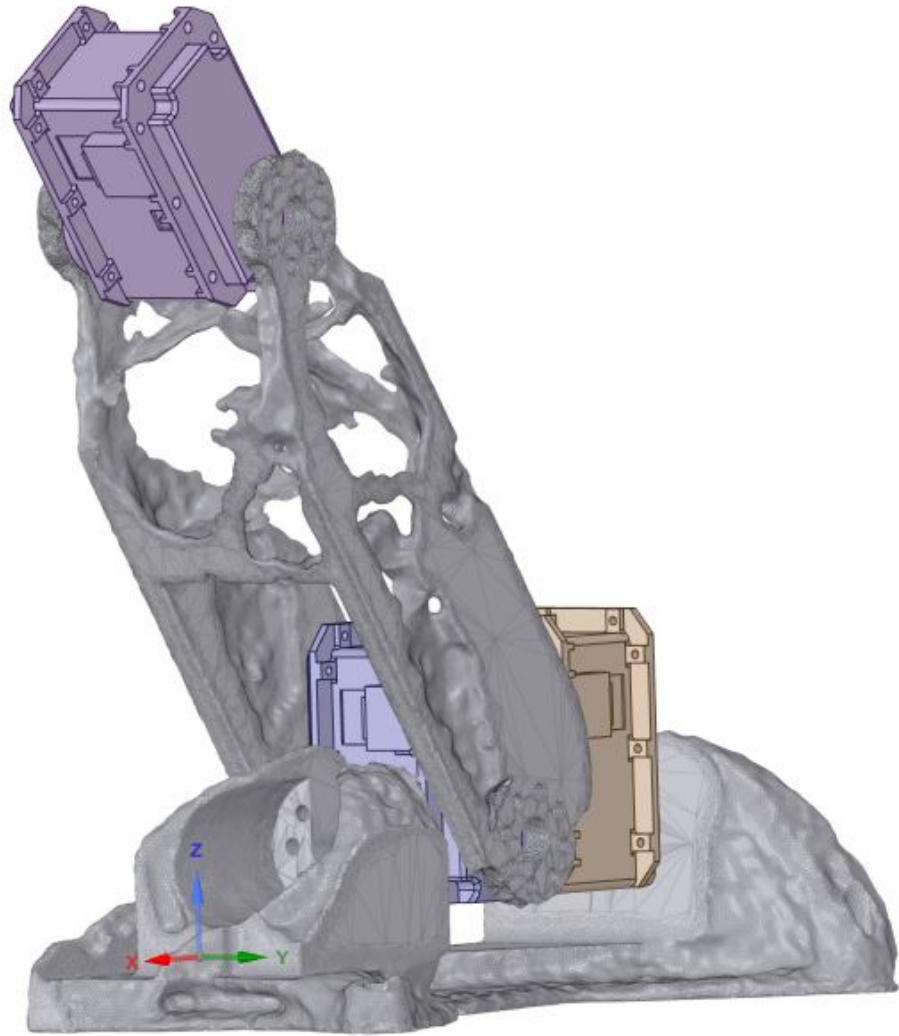


Figure 38: Models of the optimized lower leg and the optimized foot with motors

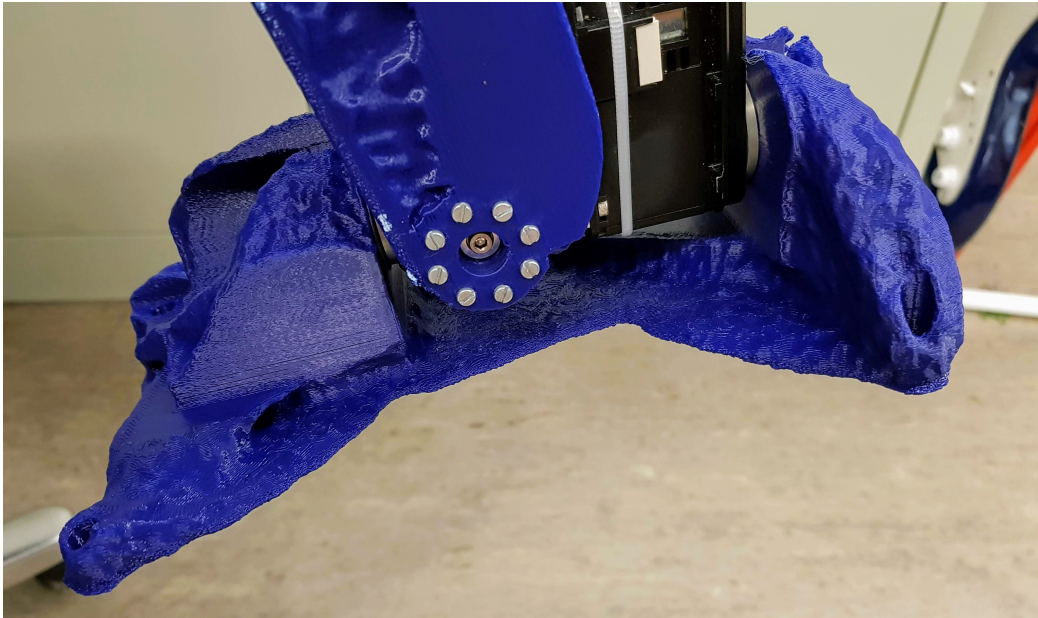


Figure 39: Side view of the printed optimized foot showing the connection to the leg

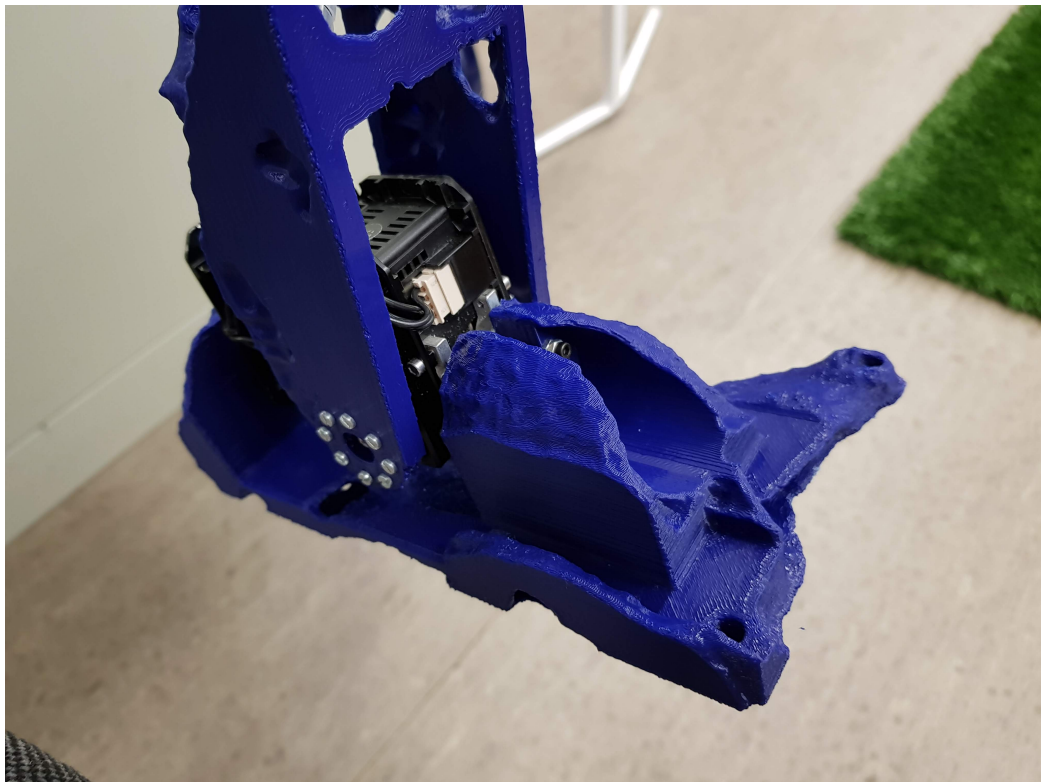


Figure 40: Front view of the printed optimized foot mounted on the optimized lower leg

5 Manufacturing the Optimized Parts using Additive Manufacturing

The corrected and smoothed parts were printed using the *Prusa i3* FDM-printer with a PLA-filament with a diameter of 1.75mm shown in Figure 41. Since the structures often contain large bridges, support material had to be generated for those sections of the 3D-model for successful prints. In order to keep the time for each print as low as possible, a configuration with rather high moving speeds was used to create the g-code for the printer. After the part was printed, the support material had to be removed, revealing the finished part as can be seen in Figure 42.

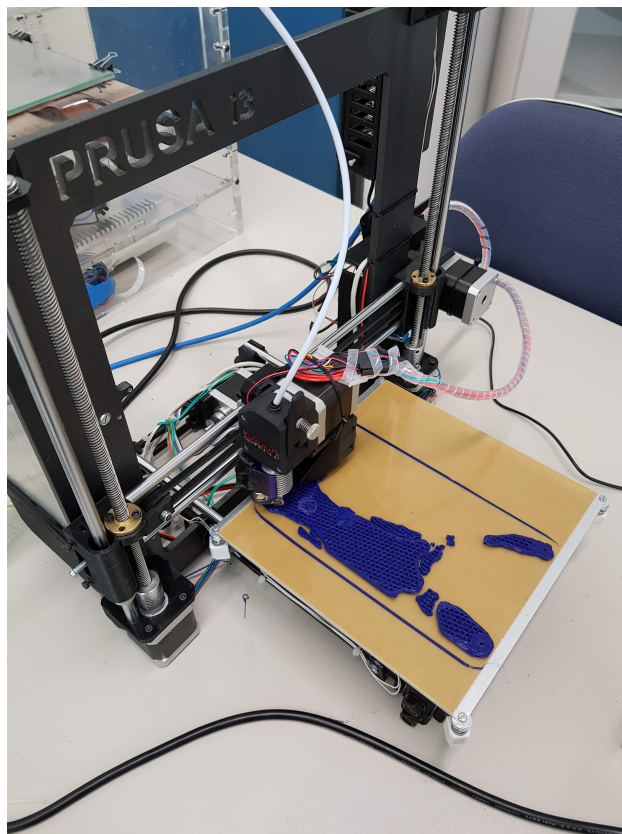


Figure 41: The Prusa i3 FDM-printer printing one of the first layers of an optimized foot



Figure 42: Printed optimized leg with support material already removed

6 Results

After some iterations, different interesting designs and shapes have been produced by the topology optimization as shown in Figures 43, 44 and 45. Each iteration step revealed different manufacturing constraints, that had to be incorporated into the design and optimization stages. The first optimized part revealed, that the thickness of the mounting faces must not be variable and therefore had to be constrained by the design. This is conditioned by the length of the M2.5 screws, used to mount the foot, which are only manufactured in specific sizes. Figure 43 shows the problematic prototype. A small amount of optimization results showed multiple disconnected parts which indicated the need for a continuity constraint. Stability wise, the



Figure 43: Printed optimized foot with screw holes of alternating depths making it impossible to mount

optimized feet performed very well in a short walking test, as they did not break or performed noticeably different from the naive approaches made from



Figure 44: Optimized foot with very thin structure connecting the front and back section

aluminum.

The weight of the feet was greatly reduced by roughly 31%, decreasing the inertia when accelerated by the robot. This paves the way for improvements to the walking algorithm, since the robot can react quicker to, for example, sensor-information. It also decreases the print time of the foot, since there is less material to be printed. A typical print job took between seven and nine hours to complete.

Contrary to the optimized foot, the optimized leg was 22% heavier than the original leg. The reason for this lies in the fact, that the original leg is mainly made from carbon-fiber parts, which simply outperform PLA. The complete construction of the lower leg including the leg, foot and the motors weighs 636g which is close to 10% less than the original weight of 702g.

In order to show that simply mirroring the parts before printing is sufficient to meet symmetry constraints, the right-leg was mounted as the left leg, showing no signs of impaired performance while walking. Figure 46 and 47 show the finished parts.



Figure 45: Optimized foot with only 15% mass retention setting mounted on the robot for a walking test

	Foot	Leg
Volume	156.40 cm^3	93.41 cm^3
Weight	184 g	86 g
Used Filament	65.02 m	38.83 m
Print Time	7 Hours 48 Minutes	8 Hours 56 Minutes

Table 3: Data about the volume, weight, used filament and print time of the optimized foot and leg of the robot

	Unaltered Leg	Optimized Leg
Weight	70 g	86 g (22% gain)
Time to obtain	Days to Weeks	<9 Hours

Table 4: Comparison of weight and the time it takes to obtain the part of the optimized and unaltered leg of the robot

	Unaltered Foot	Optimized Foot
Weight	268 g	184 g (31% reduction)
Time to obtain	Days to Weeks	<8 Hours

Table 5: Comparison of weight and the time it takes to obtain the part of the optimized and unaltered foot of the robot

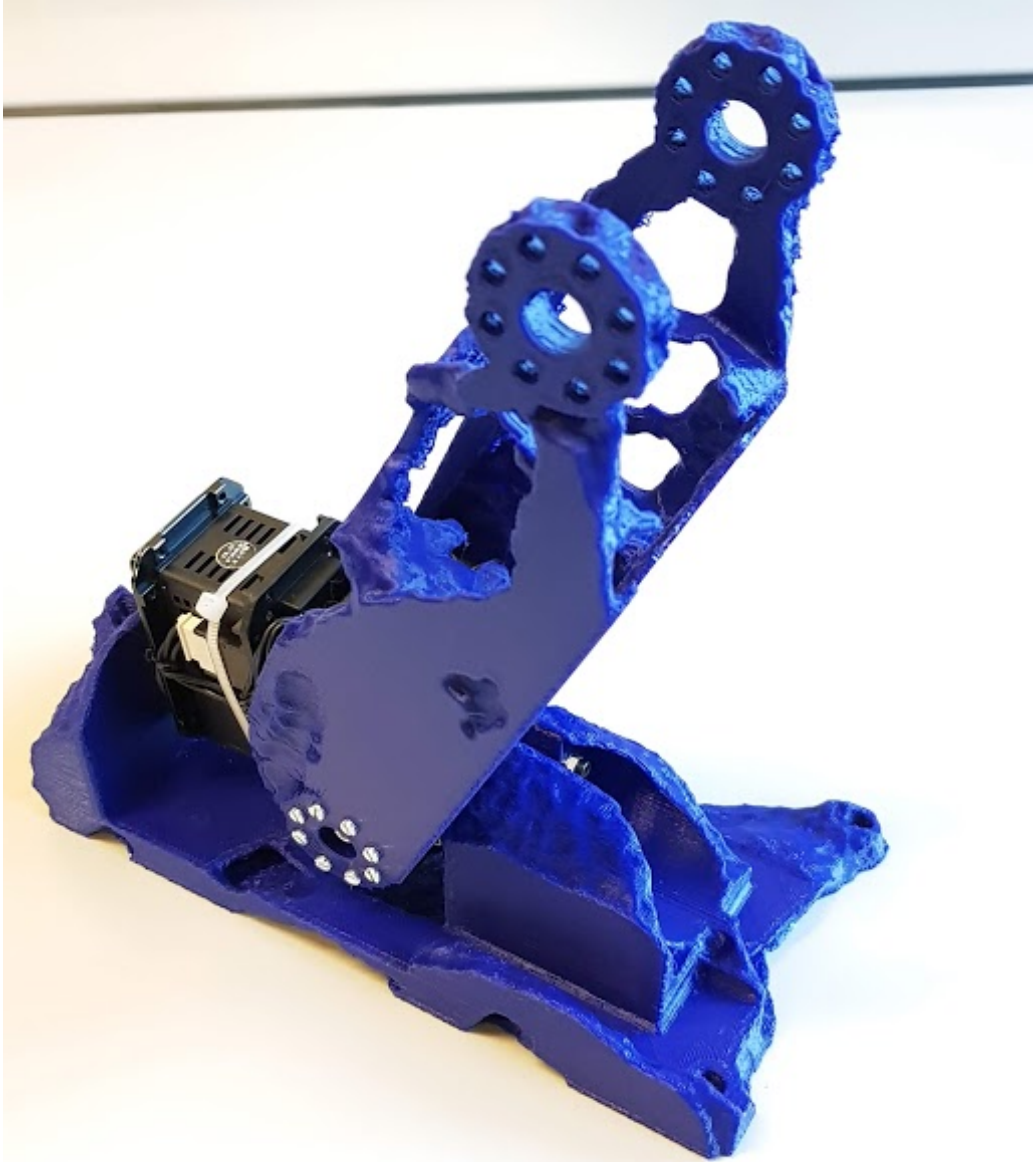


Figure 46: Optimized leg and foot mounted on the servo motors of the foot resembling a complete lower leg



Figure 47: Optimized leg and foot mounted on the robot next to an unmodified leg

7 Conclusion

When parts of a robot break, an off-site manufactured part takes days to arrive. On-site manufacturing using AM solves this problem and opens up the opportunity to re-imagine the shape and design of robotic parts. By using topology optimization to reduce the weight of parts while maintaining their stability, I was able to produce lighter parts in a much shorter time than it would take to order the parts from a third-party supplier. The parts were 3D-modeled using a software called *SpaceClaim* from the *ANSYS Workbench* suite. Forces and torques that were recorded using the *gazebo* simulation software, motor-currents of the robot as well as values from an ATI Mini45 f/t-sensor, were incorporated into a FEA and built the foundation for the topology optimization of the parts. The results were geometrically corrected and smoothed manually and then printed using a low-cost FDM 3D-printer. The finished parts were tested on the real robot and showed no obvious signs of impaired performance. The obtained shapes and designs of the parts led to further design questions such as how many supporting studs should be put under the foot of the robot. The process of printing a part took between 7 and 9 hours per part. Therefore the availability was significantly increased so that parts can be replaced on the next, if not on the same day.

7.1 Outlook

With the use of topology optimization and AM, prototyping new concepts of robotic parts can be achieved very easily. In the future this might very well lead to very efficient shapes for all parts of the robot. Especially the feet of the robot will largely benefit from the possibility to model and optimize flexible structures. This might be useful for a more springy foot and a rolling over motion of the foot while walking. Additionally the walking of the robot might also benefit from optimized topology in terms of walking speed and stability and in the distant future even in terms of aerodynamics. Ultimately these improvements will lead to a very abstract and optimal structure of the parts of the robot. Robots might very well outperform humans in various tasks.

In terms of AM, improvements in the speed and overall printing technology, will lead to even higher availability of on-site manufactured parts. New printing approaches might further lower the cost of producing parts. Finally, the need for support material will heavily decrease, or even disappear completely, allowing for even more advanced structures and designs.

References

- Berman, Barry (2012). “3-D printing: The new industrial revolution.” In: *Business horizons* 55.2, pp. 155–162.
- Bestmann, Marc, Bente Reichardt, and Florens Wasserfall (2015). “Hambot: an open source robot for RoboCup Soccer.” In: *Robot Soccer World Cup*. Springer, pp. 339–346.
- Brackett, D, I Ashcroft, and R Hague (2011). “Topology optimization for additive manufacturing.” In: *Proceedings of the solid freeform fabrication symposium, Austin, TX*. Vol. 1. S, pp. 348–362.
- Design Guide: Fused Deposition Modeling* (n.d.). Date accessed: 04.06.2018. URL: https://cdn2.hubspot.net/hubfs/340051/Design_Guides/Xometry_DesignGuide_FDM.pdf.
- TAMS (2017). *Design of a 3D-printed Humanoid Robot*. Date accessed: 22.05.2018. URL: <https://tams.informatik.uni-hamburg.de/theses/index.php?content=TopologyOptimizedRobot>.
- Finnes, Tyler (2015). “High definition 3D Printing—Comparing SLA and FDM Printing Technologies.” In: *The Journal of Undergraduate Research* 13.1, p. 3.
- Hild, Manfred, Torsten Siedel, Christian Benckendorff, Matthias Kubisch, and Christian Thiele (2012). “Myon: Concepts and design of a modular humanoid robot which can be reassembled during runtime.” In: *Field Robotics*. World Scientific, pp. 45–52.
- Hull, Charles W. (1984). *US4575330A - Apparatus for production of three-dimensional objects by stereolithography*. URL: <https://patents.google.com/patent/US4575330A/en>.
- Koenig, Nathan and Andrew Howard (2004). “Design and use paradigms for gazebo, an open-source multi-robot simulator.” In: *Intelligent Robots and Systems, 2004.(IROS 2004). Proceedings. 2004 IEEE/RSJ International Conference on*. Vol. 3. IEEE, pp. 2149–2154.
- Krog, Lars, Alastair Tucker, Martin Kemp, and Richard Boyd (2004). “Topology optimisation of aircraft wing box ribs.” In: *10th AIAA/ISSMO multidisciplinary analysis and optimization conference*, p. 4481.

- Lapeyre, Matthieu (2014). “Poppy: open-source, 3D printed and fully-modular robotic platform for science, art and education.” PhD thesis. Université de Bordeaux.
- Robotis (2009). *MX-106T / MX-106R eManual*. Date accessed: 24.07.2018. URL: http://support.robotis.com/en/product/actuator/dynamixel/mx_series/mx-106.htm.
- Palermo, Elizabeth (2013). “Fused deposition modeling: most common 3D printing method.” In: *LiveScience, Purch* 19.
- Ravi, B (2005). *Metal casting: computer-aided design and analysis*. PHI Learning Pvt. Ltd. ISBN: 8120327268.
- Sardain, Philippe and Guy Bessonnet (2004). “Forces acting on a biped robot. Center of pressure-zero moment point.” In: *IEEE Transactions on Systems, Man, and Cybernetics-Part A: Systems and Humans* 34.5, pp. 630–637.
- Sigmund, Ole and Kurt Maute (2013). “Topology optimization approaches.” In: *Structural and Multidisciplinary Optimization* 48.6, pp. 1031–1055.
- ATI Industrial Automation Manual (2016). *Six-Axis Force/Torque Sensor System - Installation and Operation Manual*. Date accessed: 18.05.2018. URL: https://www.ati-ia.com/app_content/documents/9620-05-Transducer%20Section.pdf.
- Torres, Jonathan, José Coteló, Justin Karl, and Ali P Gordon (2015). “Mechanical property optimization of FDM PLA in shear with multiple objectives.” In: *Jom* 67.5, pp. 1183–1193.
- Torries, Brian, Saber DorMohammadi, Frank Abdi, Scott Thompson, and Nima Shamsaei (2017). “Topology Optimization of an Additively Manufactured Beam.” In:
- Wang, Weiming, Tuanfeng Y Wang, Zhouwang Yang, Ligang Liu, Xin Tong, Weihua Tong, Jiansong Deng, Falai Chen, and Xiuping Liu (2013). “Cost-effective printing of 3D objects with skin-frame structures.” In: *ACM Transactions on Graphics (TOG)* 32.6, p. 177.
- Wang, Xiaojian, Shanqing Xu, Shiwei Zhou, Wei Xu, Martin Leary, Peter Choong, M Qian, Milan Brandt, and Yi Min Xie (2016). “Topological

design and additive manufacturing of porous metals for bone scaffolds and orthopaedic implants: a review.” In: *Biomaterials* 83, pp. 127–141.

Wasserfall, Florens, Norman Hendrich, Fabian Fiedler, and Jianwei Zhang (2017). “3D-Printed Low-Cost Modular Force Sensors.” In:

Zegard, Tomás and Glaucio H Paulino (2016). “Bridging topology optimization and additive manufacturing.” In: *Structural and Multidisciplinary Optimization* 53.1, pp. 175–192.

Eidesstattliche Erklärung

Hiermit versichere ich an Eides statt, dass ich die vorliegende Arbeit im Bachelorstudiengang Informatik selbstständig verfasst und keine anderen als die angegebenen Hilfsmittel – insbesondere keine im Quellenverzeichnis nicht benannten Internet-Quellen – benutzt habe. Alle Stellen, die wörtlich oder sinngemäß aus Veröffentlichungen entnommen wurden, sind als solche kenntlich gemacht. Ich versichere weiterhin, dass ich die Arbeit vorher nicht in einem anderen Prüfungsverfahren eingereicht habe und die eingereichte schriftliche Fassung der auf dem elektronischen Speichermedium entspricht.

Hamburg, den 30.07.2018

Julian Deinert

Veröffentlichung

Ich stimme der Einstellung der Arbeit in die Bibliothek des Fachbereichs Informatik zu.

Hamburg, den 30.07.2018

Julian Deinert